THE UNIVERSITY of EDINBURGH

Edinburgh Research Explorer

Multiple Jets at the LHC with High Energy Jets

Citation for published version:
R. Andersen, J & M. Smillie, J 2011, 'Multiple Jets at the LHC with High Energy Jets', *Journal of High Energy Physics*, vol. 2011, no. 6, 10. https://doi.org/10.1007/JHEP06(2011)010

Digital Object Identifier (DOI):
10.1007/JHEP06(2011)010

Link:
Link to publication record in Edinburgh Research Explorer

Document Version:
Publisher's PDF, also known as Version of record

Published In:
Journal of High Energy Physics

Publisher Rights Statement:
This article is distributed under the terms of the Creative Commons
Attribution Noncommercial License which permits any noncommercial use, distribution, and reproduction in any medium, provided the original author(s) and source are credited.

General rights
Copyright for the publications made accessible via the Edinburgh Research Explorer is retained by the author(s) and / or other copyright owners and it is a condition of accessing these publications that users recognise and abide by the legal requirements associated with these rights.

Take down policy
The University of Edinburgh has made every reasonable effort to ensure that Edinburgh Research Explorer content complies with UK legislation. If you believe that the public display of this file breaches copyright please contact openaccess@ed.ac.uk providing details, and we will remove access to the work immediately and investigate your claim.

Download date: 07. May. 2023

Published for SISSA by Springer

Received: *February 1, 2011*
Revised: *March 18, 2011*
Accepted: *May 9, 2011*
Published: *June 6, 2011*

JHEP06(2011)010

Multiple jets at the LHC with high energy jets

Jeppe R. Andersen[a] **and Jennifer M. Smillie**[b]

[a] *CP*^{3}*-Origins,*
Campusvej 55, DK-5230 Odense M, Denmark
[b] *School of Physics and Astronomy, University of Edinburgh,*
Mayfield Road, Edinburgh EH9 3JZ, U.K.

E-mail: jeppe.andersen@cern.ch, j.m.smillie@ed.ac.uk

Abstract: We present a flexible Monte Carlo implementation of the perturbative framework of *High Energy Jets*, describing multi-jet events at hadron colliders. The description includes a resummation which ensures leading logarithmic accuracy for large invariant mass between jets, and is matched to tree-level accuracy for multiplicities up to 4 jets. The resummation includes all-order hard corrections, which become important for increasing centre-of-mass energy of the hadronic collision.

We discuss observables relevant for confronting the perturbative framework with 7 TeV data from the LHC, and the impact of the perturbative corrections on several dijet and trijet observables which are relevant in the search for new physics.

Keywords: QCD Phenomenology

ArXiv ePrint: 1101.5394

© SISSA 2011

doi:10.1007/JHEP06(2011)010

Contents

1 Introduction **1**

2 All orders with high energy jets **4**
- 2.1 Dominance of the t-channel poles, and current-current scatting 4
- 2.2 All orders real corrections 7
  - 2.2.1 Dominant n-jet configurations 8
  - 2.2.2 Amplitudes and effective vertices 8
- 2.3 All orders virtual corrections 10
- 2.4 Generation and regularisation of the cross section 10

3 Matching **15**
- 3.1 Matching for FKL configurations 15
- 3.2 Matching for non-FKL configurations 18

4 Logarithmic corrections to the scale choice **19**

5 Results **21**
- 5.1 Dijet studies 22
  - 5.1.1 Rapidity and transverse momentum distributions 22
  - 5.1.2 Δy_{fb}, H_T, $s_{j_1 j_2}$ and the average number of jets 23
- 5.2 Trijet studies 25
- 5.3 Gaps between di-jets 27

6 Summary and conclusions **29**

A The building blocks for the regularised *High Energy Jets*-cross sections **30**

B Variations of the regularisation parameter λ **31**

C Stability of equal cut in the transverse momentum of dijets **32**

1 Introduction

The cross-section at the LHC for particles charged under QCD will generally be larger than that for colourless particles, and so many of the discovery channels used in the search for new physics involve the detection of hard, hadronic jets. The large mass hierarchy between any (often heavy, in order to avoid existing exclusion limits) new particle produced and those of the decay products often implies that many jets will be produced in the decay of a new state. The finger prints of any such new physics will, however, have to be found

JHEP06(2011)010

amongst a large contribution to the same signature from multi-jet processes within the Standard Model. Therefore, a detailed understanding of the Standard Model processes will assist in the search for new physics. Examples of Standard Model processes acting as background to many searches for new physics are e.g. W, Z+jets (especially with 3,4 jets or more).

However, even the nature of some Standard Model processes is best studied in events with multiple jets. For example, the CP-structure of the induced Higgs boson couplings to gluons through a top-loop could be measured by a study of the azimuthal angle between the two jets in events with a Higgs boson in association with dijets [1, 2].

In both examples, hard radiative corrections will be sizeable at the LHC, by which we mean that the exclusive $(n+1)$-jet rate is a significant component of the inclusive n-jet rate. And more so in many of the regions of interest for searches of new physics. Therefore, a tree-level description of the inclusive n-jet process will be unsatisfactory for the involved analyses beyond just a measurement of the cross section.

The reason for the increased importance in many situations of hard, perturbative corrections at the LHC over the situation at previously, lower energy colliders is very simple. Two effects act to suppress hard corrections: the increasing powers of the perturbative coupling, and the increase in the light-cone momentum fraction of the partons extracted from the proton beyond that necessary for the final state without the additional hard jet. The suppression from this last kinematic effect is caused by the decrease in the parton density functions (pdf) as the light-cone momentum fraction x is increased. However, for processes with at least two particles in the final state, there is a fine trade-off between the suppression from the pdf and the increasing phase space for additional emission in-between the most forward/backward hard jet (even when this additional emission is hard in transverse momentum), as the rapidity span between the two most forward/backward jets is increased. At previous, lower-energy colliders, this balance was tipped more towards a suppression than will be the case at the LHC.

At previous colliders, the "significant" rapidity separation of the two objects, which is necessary for the opening of phase space for additional radiation, would already bring the light-cone momentum fractions into the region of extremely fast falling pdfs as $x \to 1$, thus effectively vetoing additional emissions. However, the situation is different for the LHC processes discussed above, since in the case of e.g. W-boson production with at least 3 jets, two jets will naturally be produced with a size-able separation in rapidity [3]. In this case, there is only a small suppression for additional (especially central) radiation, even when the additional jets have a sizeable transverse momentum. This holds true also for other processes, provided the hard scattering amplitude has a mechanism for effectively radiating into the rapidity span. This is the case when colour is exchanged between the particles either side of the span, whereas a colour-singlet exchange leads to less radiation in the span [4, 5].

While a fixed order (e.g. LO or NLO) calculation may be adequate for the description of sufficiently inclusive quantities like the total inclusive cross section, the question is to what extent a given theoretical description allows for the radiation into the phase space which becomes available with the increase in partonic centre of mass energy — and how important the description of this radiation is for a given observable. The current paper

JHEP06(2011)010

discusses these problems, and presents results obtained in a recently proposed all-order perturbative framework.

It is clear that a NLO calculation allows for just one, also hard, additional emission above the minimum number of jets required in the analysis. The all-order description of a parton shower, on the other hand, captures the soft and collinear emissions, but will underestimate the amount of hard radiation. This deficiency can be repaired order-by-order through a CKKW-L-style matching [6–8], or to full NLO accuracy [9, 10] for low multiplicities. In both cases, the deficiency of the parton shower in describing hard radiation is repaired by the use of full tree-level matrix elements. The maximum multiplicity applied in the tree-level matching is limited by the time for evaluation of the tree-level matrix elements. Since in a CKKW-L-style analysis the matching scale should be chosen somewhat smaller than the transverse scale required in the definition of jets to avoid matching artefacts, the matching procedure will run out of available matrix elements at a lower multiplicity than the maximum for which the LO process has been calculated. This can be viewed simply as a result of the attempt within the matching procedure to describe not just the total rate, but also the final state configuration.

The framework of *High Energy Jets* (HEJ) [11, 12] provides an all-order description of processes with more than two hard jets, based on an approximation which captures the hard, wide-angle emissions missed in a shower-approach based on soft and collinear splitting functions. HEJ does not try to redo the job of the shower, but focuses specifically on the part *not* done by a parton shower. Work is in progress to combine the description of HEJ with a parton shower [13]; the most important component of the matching between HEJ and a parton shower is the avoidance of double counting of soft radiation, which is treated to all orders in both descriptions.

The formalism of HEJ is inspired by that underlying [14–16] the BFKL equation [17], and as such, an approximation for both real and virtual corrections is obtained to all orders, obviously with all IR divergences cancelling between the two contributions. Differently to the BFKL approach, however, HEJ applies an approximation only to the partonic scattering amplitudes, and not the phase space integration, which is performed for each explicit multiplicity. In this respect, HEJ resembles a parton shower formulation of an all-order summation. Furthermore, by applying the approximations at the level of the scattering amplitude $\mathcal{M}$ (and not $|\mathcal{M}|^2$), it is possible to supplement [11, 12] the approximations with the requirement of e.g. gauge invariance, and thereby obtain a formalism, which reproduces more accurately the fixed order perturbative results when checked order by order, while simultaneously being sufficiently simple that all-order results can be explicitly obtained.

In the current paper, we develop further the formalism of High Energy Jets by matching to fixed order results and include some sub-leading corrections. Furthermore, we demonstrate the application of HEJ to the production of at least two and at least three jets.

The structure of the paper is as follows: in section 2 we briefly review the formalism within *High Energy Jets*, which allows approximate all-order results to be obtained [11, 12]. In section 3 we describe the matching of these amplitudes to full, high-multiplicity tree-level results. In section 4 we include some sub-leading corrections, which stabilise the dependence on the scale choice [18, 19]. In section 5 we present results for dijet production

JHEP06(2011)010

obtained with the full formalism of *High Energy Jets*, and discuss observables and distributions for which the higher-order corrections are particularly important in order to obtain a perturbatively stable description. These can lead to a direct experimental test of the importance of the correct perturbative description.

The all-order results presented in this paper are obtained using the implementation of the formalism of *High Energy Jets* in a fully flexible parton-level Monte Carlo generator, which can be downloaded at http://cern.ch/hej.

2 All orders with high energy jets

The all-order perturbative framework of *High Energy Jets* (*HEJ*) initiated in ref. [11, 12, 20, 21] is addressing some of the short-comings in the description of multiple hard, perturbative corrections in both the (low) fixed-order and in the parton shower formulation. The perturbative description obtained with *HEJ* reproduces the correct, all-order, full QCD limit for both real and virtual corrections to the hard perturbative matrix element for the hard, wide-angle emissions which underpin the perturbative description of the formation of additional jets. The central parts of the formalism were presented in ref. [11, 12] and discussed further in ref. [22, 23]. In this section, we will give just a brief overview of the formalism on which the approximations are based; the next section will then discuss how to incorporate matching corrections to full, high multiplicity tree-level accuracy.

2.1 Dominance of the t-channel poles, and current-current scatting

In the standard parton shower formalism, the physical picture is one of successive branchings off s-channel propagators, governed by the DGLAP splitting functions [24–27]. Such a framework can sum to leading logarithmic accuracy, and to all orders the behaviour dictated by the *soft* and *collinear* s-channel singularities arising in the perturbative corrections to a given scattering amplitude. It describes correctly emissions with small invariant mass to the hard scattering amplitude.

The limit of pure N-jet amplitudes for *large* invariant mass between each parton of similar transverse momentum is described by the FKL-amplitudes [14, 15], which are at the foundation of the BFKL framework [17]. The physical picture arising from the FKL amplitudes is one of effective vertices connected by t-channel propagators. The reduction of the formalism to the two-dimensional BFKL integral equation relies on many kinematical approximations, which are extended to all of phase space. Using an explicit (or so-called iterative) solution to the BFKL equation [28–30], it is however straightforward to show that despite the logarithmic accuracy (in $\hat{s}/\hat{t}$), the perturbative expansion of the (B)FKL solution does not give a satisfactory description of the results obtained order by order with the true perturbative series from QCD [21].

High Energy Jets [11, 12] inherits the idea of effective vertices connected by t-channel currents in order to reproduce the correct limit of N-jet amplitudes, but goes beyond controlling just the logarithmic accuracy like the FKL formalism. The kinematic building blocks of the FKL formalism depend on transverse momenta only, as a result of the

JHEP06(2011)010

kinematic limits applied in order to separate the amplitude into effective vertices separated by t-channel exchanges [31]. In the following, we will discuss how to obtain a better approximation for the t-channel singularities.

The $2 \to 2$ scattering $qQ \to qQ$ obviously proceeds through just a t-channel exchange of the gluon current generated by a quark. A good formalism for the description the t-channel poles should get at least this very simple process exact. The colour and helicity averaged and summed square of this simple scattering amplitude is given by

$$|\overline{\mathcal{M}}^{\text{tree}}_{qQ\to qQ}|^2 = g^4 \ \frac{4}{9} \ \frac{s^2+u^2}{t^2}. \tag{2.1}$$

Despite its simplicity, this amplitude can already be used to illustrate the problem of the approximations made in the standard BFKL procedure. The limit of *Multi-Regge-Kinematics* is defined for the scattering process $p_A, p_B \to p_1, \ldots, p_n$ in terms of transverse momenta and rapidities $y = \ln\left(\frac{E+p_z}{E-p_z}\right)$ as the following conditions

$$\forall i \in \{2, \ldots, n-1\} : y_{i-1} \gg y_i \gg y_{i+1}, \quad \forall i,j : |p_{i\perp}| \approx |p_{j\perp}|, \tag{2.2}$$

or alternatively

$$\forall i,j : |p_{i\perp}| \approx |p_{j\perp}|, \quad s_{ij} \to \infty, \tag{2.3}$$

where $s_{ij} = 2\ p_i.p_j$ and $s = 2\ p_A.p_B$. For the $2 \to 2$ process, the MRK limit of the Mandelstam variables is given by $t \to -k_\perp^2$, $s \approx -u \to \infty$. The effective approximation applied in the BFKL formalism (both at LL and NLL) for the $2 \to 2$ process is $|\overline{\mathcal{M}}^{\text{BFKL,Tree}}_{qQ\to qQ}|^2 = g^4 \ \frac{8}{9} \ s^2/(k_\perp^2)^2$. However, for much of the kinematics relevant at the LHC, t and $-k_\perp^2$ differ by at least an order of magnitude, and s and u differ significantly, leading to a gross overestimation of the cross section, if the BFKL approximation is applied.

In eq. (2.1), the s^2-component arises from scattering of quarks of the same helicities (e.g. $q^-Q^- \to q^-Q^-$), whereas the u^2-component arises from the scatting of unlike helicities (e.g. $q^-Q^+ \to q^-Q^+$). Since this difference is important in obtaining sufficient accuracy, *HEJ* is based on the calculation of scattering processes at the amplitude level (as opposed to the square of the amplitude), and the sum over helicities is performed explicitly. For the qQ-process then, the obvious choice of formalism is that of current-current scattering.

In the spinor notation for the quark currents (see ref. [11] for details), $j^{-\mu}_{a1} = \bar{u}^-_1 \gamma^\mu u^-_a$ is written as $\langle 1|\mu|a\rangle$, and then the (colour and coupling stripped) matrix element for the process $q^-_{p_a} Q^-_{p_b} \to q^-_{p_1} Q^-_{p_2}$ reads

$$M_{q^-Q^-\to q^-Q^-} = \ \langle 1|\mu|a\rangle \frac{g^{\mu\nu}}{t} \langle 2|\nu|b\rangle. \tag{2.4}$$

While it is possible to shorten this expression by use of the Fierz identity, we choose to keep the formulation in terms of currents, as this will prove useful for the generalisation to other processes, including W, H, Z+jets.

Let us denote the spinor string (for helicities h_a, h_1, h_b, h_2 of the quarks) appearing in the amplitude as

$$S^{h_a h_b \to h_1 h_2}_{qQ\to qQ} = \langle 1\ h_1|\mu|a\ h_a\rangle\ g^{\mu\nu}\ \langle 2\ h_2|\nu|b\ h_b\rangle. \tag{2.5}$$

JHEP06(2011)010

This complex number can be calculated using any explicit representation for the spinors (see e.g. ref. [11, 12]), and we will denote the sum over helicities of the absolute square of this number by

$$\|S_{qQ\to qQ}\|^2 = \sum_{h_a,h_a,h_b,h_2} \left|S^{h_a h_b\to h_1 h_2}_{qQ\to qQ}\right|^2. \tag{2.6}$$

Of course in this case non-zero contributions arise only when $h_a = h_1$ and $h_b = h_2$.

The colour and helicity summed and averaged matrix element for the scattering process $qQ \to qQ$ is then

$$\begin{aligned}\overline{|\mathcal{M}_{qQ\to qQ}|}^2 &= \frac{1}{4\ (N_C^2-1)}\ \|S_{qQ\to qQ}\|^2 \\ &\cdot \left(g^2\ C_F\ \frac{1}{t_1}\right) \\ &\cdot \left(g^2\ C_F\ \frac{1}{t_2}\right).\end{aligned} \tag{2.7}$$

with $t_1 = (p_a - p_1)^2$ and $t_2 = (-p_b + p_2)^2$ (obviously $t_1 = t_2$ in this case of a $2 \to 2$-process), which equals eq. (2.1).

The point of this tour de force through the simple formalism of qQ-scattering is that using this formalism, the amplitudes for qg-scattering can be recast in a very similar form. In fact, a careful analysis [12] of the helicity structure in $qg \to qg$-scattering reveals that all the amplitudes where the helicity of the gluon is unchanged[1] factorise again into two currents contracted over a t-channel pole. For example, the fully colour-dressed scattering amplitude for the process $q^-(p_a) + g^+(p_b) \to q^-(p_1) + g^+(p_2)$ equals [12]

$$\mathcal{M}_{q^-g^+\to q^-g^+} = -ig^2\ \frac{p^*_{2\perp}}{|p_{2\perp}|}\left(t^2_{ea}t^b_{1e}\sqrt{\frac{p_b^-}{p_2^-}} - t^b_{ea}t^2_{1e}\sqrt{\frac{p_2^-}{p_b^-}}\right)\langle 1|\mu|a\rangle\ \frac{g^{\mu\nu}}{t}\ \langle b|\nu|2\rangle, \tag{2.8}$$

with $p_\perp = p_x + i\ p_y$, $p^- = E - p_z$. We have taken the negative z-direction to be that of the incoming gluon, without loss of generality. We immediately recognise the kinematic structure (in terms of currents) of q^-Q^+-scattering, multiplied by a momentum-dependent colour factor. The colour summed and averaged scattering matrix element is

$$\begin{aligned}|\mathcal{M}_{q^-g^+\to q^-g^+}|^2 &= \frac{1}{N_C^2-1}\ |\langle b|\rho|2\rangle\langle 1|\rho|a\rangle|^2 \\ &\cdot \left(g^2\ C_F\ \frac{1}{t_1}\right) \\ &\cdot \left(g^2\ \left[\frac{1}{2}\ \frac{1+z^2}{z}\ \left(C_A - \frac{1}{C_A}\right) + \frac{1}{C_A}\right]\ \frac{1}{t_2}\right),\end{aligned} \tag{2.9}$$

where $z = p_2^-/p_b^-$ (and again $t_1 = (p_a - p_1)^2 = (p_b - p_2)^2 = t_2$). This has a striking similarity to the amplitude for qQ-scattering (see eq. (2.7)). In fact, it differs only by the

[1] All helicity-flip amplitudes are identically zero.

JHEP06(2011)010

slightly more complicated colour factor in square brackets, which replace the C_F in the case of quark scattering. In the MRK limit $p_2^- \to p_b^-$ this tends to C_A, and the qg scattering matrix element is equal to the one for qQ rescaled by C_A/C_F, just as expected [32]. Eq. (2.9) is, however, the exact result, and the square bracket is strictly larger than C_A, and uniformly decreasing for increasing z. Small z here reflects a large change in light-cone momentum for the gluon, and unsurprisingly a strong acceleration is reflected in an effectively stronger interaction (though this is unrelated to the higher order perturbative effect of the running of the coupling).

The perhaps most interesting result of using the formalism of currents directly is the obvious display that this process has *just a t-channel pole* (i.e. no poles in the s or u-channel), exactly like the seemingly simpler qQ-scattering process. The pure t-channel structure, and the same colour factors, hold true for *all* the helicity assigments which give a non-zero contribution.

In the case of pure gluon scattering, it could seem a little arbitrary to discuss the s, t, and u-channels. However, in the cases of scattering of two gluons of opposite helicities, like $g^- g^+ \to g^- g^+$ it turns out again that *the scattering amplitude has just a t-channel pole*, and is again just the contraction of two currents with special colour factors, which depend only on the acceleration of each gluon during the scattering.

The brief summary presented here of the studies in ref. [11, 12, 22, 23] illustrates how the t-channel exchange is completely well-defined (for $2 \to 2$ processes) not just for qQ-scattering, but also for scattering processes involving gluons. This is displayed in a formalism based on helicity amplitudes and currents, without resorting to kinematic approximations or limits.

2.2 All orders real corrections

The previous section demonstrated that the t-channel pole of the full scattering amplitudes is much more important for the accurate description of the scattering processes than the zoo of Feynman diagrams would suggest. We demonstrated how this t-channel pole can be described exactly for many processes by a formalism based on the scattering of specific helicity currents. For example, the colour summed and averaged amplitudes for both $qQ \to qQ$ and $qg \to qg$ scattering are described exactly by a formalism of pure quark current scatterings, with colour factors depending on the flavour (quark or gluon) of the scattered partons.

In the current section we will describe briefly the approximations to the real, radiative corrections of the $2 \to 2$ process in *High Energy Jets*. The soft and collinear regions are already well understood by the description in a parton shower. HEJ focuses instead on the hard, radiative corrections. The aim is to build a framework which is sufficiently accurate for a "first guess" for the impact of the radiative corrections (i.e. to all order with a certain logarithmic accuracy), but which then is also sufficiently flexible to include matching to the full fixed-order result, where this is accessible. The control of the cross section to leading logarithmic accuracy in $\log(s/t)$ requires control of the hard scattering matrix element to leading power in s/t, as $s/t \to \infty$. As discussed in the previous section, and in more depth in e.g. ref. [11, 12, 21], the control of the leading power alone is achieved already

JHEP06(2011)010

in the formalism of Fadin-Kuraev-Lipatov [14–16], but this is insufficient to ensure a good description of the scattering amplitudes in the energy regime of the LHC. The formalism described here combines the right limit at $s/t \to \infty$ (or more generally the MRK limit) with complete gauge-invariance. It is already clear that the description of the $2 \to 2$-processes discussed in the previous section is gauge invariant, since it describes the t-channel pole of the full scattering amplitude exactly. In the current section we will build a gauge-invariant approximation to $2 \to n$-processes.

2.2.1 Dominant n-jet configurations

First, we will discuss briefly which processes dominate the $2 \to n$ partonic scattering in the MRK limit. For any $2 \to n$ scattering process, the final state particles can obviously be ordered according to rapidity. Apart from exceptional phase space points (of zero measure), no two particles will have the same rapidity.

At the currently implemented accuracy, the HEJ amplitudes will describe the leading contribution (in the invariant mass between two neighbouring partons) to the n-jet production process. For a given n-jet kinematic configuration, many of the possible partonic channels will be systematically suppressed. These channels will not be summed to all orders, but will be included "only" through matching corrections. Consider now the rapidity ordered final state jets. The leading contributions to the n-jet configurations are those where the flavour of the most forward jet equals that of the incoming parton of positive light-cone momentum, and the flavour of the most backward jet is identical to that of the incoming parton of negative light-cone momentum. The leading contribution to jet production between the jets extremal in rapidity is given by pure gluon emissions. Such processes can proceed through a gluon exchange between all rapidity-ordered particles. Changing the flavours of two jets, such that a single gluon propagator between the two jets is replaced by a t-channel quark propagator, automatically leads to a suppression of $1/s_{ij}$ for $s_{ij} \to \infty$, where s_{ij} is the invariant mass between the two jets. We choose to call the leading configurations *FKL*-configurations, since they are the same as those which are considered in the amplitudes by Fadin-Kuraev-Lipatov [14–16, 33–35].

2.2.2 Amplitudes and effective vertices

The all-order approximations of the n-parton FKL-configurations are constructed similarly to the $2 \to 2$ scattering amplitudes considered in section 2.1, as effective vertices connected by t-channel propagators. In the case of the partons of largest or smallest rapidity, these are directly the effective currents discussed in the previous section. The emission of additional gluons is performed by gauge-invariant,[2] effective vertices. These were derived in ref. [11], and take into account the leading contribution from emissions off both the t-channel exchange and the two incoming and the most forward/backward outgoing partons. The effective vertex for the emission of a gluon of momentum $p_g = q_1 - q_2$, $V^\mu(q_i, q_{i+1})$, is

[2] by which we of course mean fully gauge invariant, not just up to sub-asymptotic terms as it is often meant in the BFKL literature.

JHEP06(2011)010

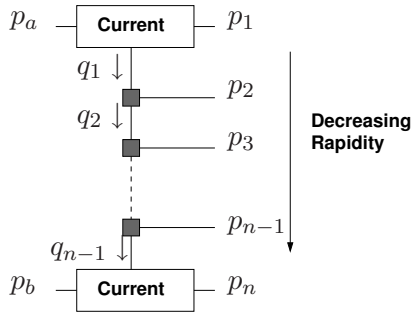

Figure 1. The analytic structure of a scattering amplitude in *High Energy Jets*.

given by [11]

$$\begin{aligned} V^\rho(q_i, q_{i+1}) = &- (q_i + q_{i+1})^\rho \\ &+ \frac{p_A^\rho}{2}\left(\frac{q_i^2}{p_{i+1}\cdot p_A} + \frac{p_{i+1}\cdot p_B}{p_A\cdot p_B} + \frac{p_{i+1}\cdot p_n}{p_A\cdot p_n}\right) + p_A \leftrightarrow p_1 \\ &- \frac{p_B^\rho}{2}\left(\frac{q_{i+1}^2}{p_{i+1}\cdot p_B} + \frac{p_{i+1}\cdot p_A}{p_B\cdot p_A} + \frac{p_{i+1}\cdot p_1}{p_B\cdot p_1}\right) - p_B \leftrightarrow p_n. \end{aligned} \tag{2.10}$$

This form of the effective vertex is fully gauge invariant; the Ward Identity, $p_g \cdot V = 0$ can easily be checked. This allows for a meaningful approximation to the scattering amplitude to be constructed.

Another approximation of HEJ is then the systematic omission of interference effects between identical particles, since such effects are suppressed by the invariant mass between the particles. Essentially, each emission is treated as a distinguishable particle, just like in a parton shower. The resulting tree-level approximation for a $2 \to n$ scattering is illustrated in figure 1. Virtual corrections modify the t-channel propagators and are discussed together with regularisation in the next section. The tree-level HEJ-approximation for the square of the amplitude describing a qQ-scattering process with n jets in the final state is then given by [11]

$$\begin{aligned} \left|\overline{\mathcal{M}}^t_{qQ\to qg\ldots gQ}\right|^2 = &\frac{1}{4\ (N_C^2-1)}\ \left\|S_{qQ\to qQ}\right\|^2 \\ &\cdot \left(g^2\ C_F\ \frac{1}{t_1}\right)\cdot\left(g^2\ C_F\ \frac{1}{t_{n-1}}\right) \\ &\cdot \prod_{i=1}^{n-2}\left(\frac{-g^2 C_A}{t_i t_{i+1}}\ V^\mu(q_i, q_{i+1}) V_\mu(q_i, q_{i+1})\right), \end{aligned} \tag{2.11}$$

where $\left\|S_{qQ\to qQ}\right\|^2$ indicates the square of pure current-current scattering of section 2.1. In the case of scattering of gluons, the terms in this sum are weighted with helicity-dependent colour factors [12], one of which is listed in eq. (2.9). All the building blocks for constructing the *High Energy Jets*-scattering amplitudes are listed in appendix A.

JHEP06(2011)010

2.3 All orders virtual corrections

The virtual corrections are approximated with the *Lipatov ansatz* for the t-channel gluon propagators (see ref. [11] for more details). The *Lipatov Ansatz* states that order by order, the leading logarithmically virtual corrections to the full n-parton scattering amplitude in the MRK limit can be obtained by the following replacement in the scattering amplitudes:

$$\frac{1}{t_i} \;\to\; \frac{1}{t_i}\,\exp\left[\hat{\alpha}(q_i)(y_{i-1}-y_i)\right] \tag{2.12}$$

with

$$\hat{\alpha}(q_i) = -g^2\,C_A\,\frac{\Gamma(1-\varepsilon)}{(4\pi)^{2+\varepsilon}}\frac{2}{\varepsilon}\left(\mathbf{q}^2/\mu^2\right)^{\varepsilon}. \tag{2.13}$$

This ansatz for the exponentiation of the virtual corrections in the appropriate limit of the n-parton scattering amplitude has been proved to even the sub-leading level [31, 36–38]. In section 4 we will discuss parts of the next-to-leading logarithmic corrections, which can be included as corrections of the type $\beta_0 \log(Q^2/\mu^2)$.

2.4 Generation and regularisation of the cross section

We will now discuss the construction of the all-order, regularised dijet cross section. The necessary details for constructing a generator were already given in ref. [11, 21], but the discussion here is more detailed. We begin by defining the matrix element squared built from the t-channel factorised picture (eq. (2.11)) combined with the virtual corrections discussed in the previous section:

$$\begin{aligned}\overline{\left|\mathcal{M}^{t,v}_{\varepsilon\; f_1 f_2\to f_1 g\cdot g f_2}\right|}^2 = {}& \frac{1}{4\,(N_C^2-1)}\;\left\|S_{f_1 f_2\to f_1 f_2}\right\|^2 \\ & \cdot\left(g^2\;K_{f_1}\;\frac{1}{t_1}\right)\cdot\left(g^2\;K_{f_2}\;\frac{1}{t_{n-1}}\right) \\ & \cdot\prod_{i=1}^{n-2}\left(\frac{-g^2 C_A}{t_i t_{i+1}}\;V^{\mu}(q_i,q_{i+1})V_{\mu}(q_i,q_{i+1})\right) \\ & \cdot\prod_{j=1}^{n-1}\exp\left[2\hat{\alpha}(q_j)(y_{j-1}-y_j)\right],\end{aligned} \tag{2.14}$$

where f_1, f_2 indicate the flavour (quarks or gluon), $S_{f_1 f_2\to f_1 f_2}$ is the sum of contracted currents, and K_{f_1} is C_F if $f_1 = q$ and C_A if $f_1 = g$. These pieces are all given explicitly in appendix A.

The dijet inclusive cross section is simply constructed as the explicit phase space integral over the explicit sum of real, radiative corrections, including the leading, all-order virtual corrections. We illustrate the procedure with qQ-scattering, but the generalisation to incoming gluons is straightforward using the gluon currents and factors detailed in

JHEP06(2011)010

appendix A.

$$\sigma_{qQ\to 2j} = \sum_{n=2}^{\infty} \prod_{i=1}^{n} \left(\int \frac{\mathrm{d}^2\mathbf{p}_{i\perp}\ \mathrm{d}y_i}{2\ (2\pi)^3} \right) \frac{\overline{\left|\mathcal{M}^{t,v}_{\varepsilon\ f_1 f_2 \to f_1 g \cdot g f_2}\right|}^2}{\hat{s}^2}\ x_a f_{A,q}(x_a, Q_a)\ x_2 f_{B,Q}(x_b, Q_b) \\ \times (2\pi)^4\ \delta^2\left(\sum_{k=1}^{n} \mathbf{p}_{k\perp} \right)\ \mathcal{O}_{2j}(\{p_i\}). \tag{2.15}$$

Here, $(p_{i\perp}, y_i)$ denote the transverse momentum and rapidity of the i'th final state parton. The parton momenta fractions are given by

$$x_a = \sum_i \frac{|p_{i\perp}|}{\sqrt{s}} \exp(-y_i), \qquad x_b = \sum_i \frac{|p_{i\perp}|}{\sqrt{s}} \exp(y_i), \tag{2.16}$$

with $\sqrt{s}$ the total hadronic centre-of-mass energy. In eq. (2.15), $\sqrt{\hat{s}}$ denotes the total partonic centre-of-mass energy, $\hat{s} = x_a x_b s$, and $f_{A,q}(x_a, Q_a), f_{B,Q}(x_B, Q_B)$ denote the relevant parton density functions for parton A, B respectively at the resolution scales Q_A, Q_B. We will discuss the choices of scales further in section 4. The function $\mathcal{O}_{2j}(\{p_i\})$ takes as arguments all the final state partons, and returns 1 if there are at least two jets, according to the chosen jet-definition. It is otherwise zero. In the current study, we choose to apply the anti-kt algorithm as implemented in FastJet [39], with a R-parameter of 0.6; however, obviously any jet-definition can be applied on the partonic ensemble.

The integration over transverse momentum runs from 0 to infinity. We choose to generate only the rapidity ordered phase space (i.e. $y_{i-1} < y_i < y_{i+1}$) using the approach of ref. [40], since the *HEJ*-amplitudes $\overline{|\mathcal{M}^{t,v}_{\varepsilon}|}^2$ take as argument the rapidity ordered set $\{p_i\}$. The phase space integration of standard fixed-order amplitudes can be done in a similar way (and indeed is done in the matching-procedure of section 3), where then an additional Monte Carlo sampling is performed over the identification between the particle leg and the rapidity ordered set of momenta. The phase space generation method of ref. [40] is very efficient for processes dominated by t-channel poles.

The matrix elements $\overline{|\mathcal{M}^{t,v}_{\varepsilon}|}^2$ are divergent for any $p_{i\perp} \to 0$. We will first discuss how for all but the extremal partons, this divergence cancels with the pole in ε from the virtual corrections implemented according to the Lipatov Ansatz for the resummed t-channel propagators (we will then return to the case of the extremal partons below).

Consider the limit where the transverse momentum of the ith emitted gluon is vanishing. In this limit,

$$\overline{\left|\mathcal{M}^{t,v}_{\varepsilon\ p_a\ p_b \to p_1\ \cdots\ p_{i-1}\ p_i\ p_{i+1}\ \cdots\ p_n}\right|}^2 \overset{\mathbf{p}_i{}^2 \to 0}{\longrightarrow} \left(\frac{4\ g^2\ C_A}{\mathbf{p}_i{}^2} \right) \overline{\left|\mathcal{M}^{t,v}_{\varepsilon\ p_a\ p_b \to p_1\ \cdots\ p_{i-1}\ p_{i+1}\ \cdots\ p_n}\right|}^2, \tag{2.17}$$

where the matrix element on the r.h.s. has $n-1$ final state particles, and $\mathbf{p}_i^2$ is the sum of the squares of the transverse components of p_i in the Euclidean metric. By integrating

JHEP06(2011)010

over the soft region $\mathbf{p}_i^2 < \lambda^2$ of phase space in $D = 4 + 2\varepsilon$ dimensions we find

$$\begin{aligned}\int_0^\lambda \frac{\mathrm{d}^{2+2\varepsilon}\mathbf{p}\ \mathrm{d}y_i}{(2\pi)^{2+2\varepsilon}\ 4\pi}\left(\frac{4g^2C_A}{\mathbf{p}^2}\right)\mu^{-2\varepsilon} \\ = \frac{4g^2C_A}{(2\pi)^{2+2\varepsilon}4\pi}\Delta y_{i-1,i+1}\frac{\pi^{1+\varepsilon}}{\Gamma(1+\varepsilon)}\frac{1}{\varepsilon}(\lambda^2/\mu^2)^\varepsilon.\end{aligned} \tag{2.18}$$

The square of the matrix element on the left hand side of eq. (2.17) contains the exponential $\exp(2\hat{\alpha}(q_i)\Delta y_{i-1,i+1})$. By expanding the exponential to first order in g^2 and in ε, the resulting pole in ε does indeed cancel that of eq. (2.18), and the combined effect of one soft real emission and the first term in the expansion of the Reggeised propagator is a factor

$$\Delta y_{i-1,i+1}\frac{\alpha_s N_C}{\pi}\ln\left(\frac{\lambda^2}{\mathbf{q}^2}\right) \tag{2.19}$$

multiplying the $(n-1)$-particle matrix element. It is clear that the nested rapidity integrals of additional soft radiation in the t-channel factorised multi-parton amplitudes will build up the exponential needed to cancel the poles from the virtual corrections to all orders in α_s. The divergence arising from a given real emission is therefore cancelled by that arising from the virtual corrections in the Reggeised t-channel propagator of the matrix element without the relevant real emission. Therefore, if indeed eq. (2.17) had been an equality for $p_i^2 < \lambda^2$, then the regularised HEJ matrix element squared would be:

$$\begin{aligned}\overline{|\mathcal{M}^{\mathrm{reg}}(\{p_i\})|}^2 = \frac{1}{4\ (N_C^2-1)}\ \|S_{f_1f_2\to f_1f_2}\|^2 \\ \cdot\left(g^2\ K_{f_1}\ \frac{1}{t_1}\right)\cdot\left(g^2\ K_{f_2}\ \frac{1}{t_{n-1}}\right) \\ \cdot\prod_{i=1}^{n-2}\left(\frac{-g^2C_A}{t_it_{i+1}}\ V^\mu(q_i,q_{i+1})V_\mu(q_i,q_{i+1})\right) \\ \cdot\prod_{j=1}^{n-1}\exp\left[\omega^0(q_j,\lambda)(y_{j-1}-y_j)\right], \\ \omega^0(q_j,\lambda) = -\frac{\alpha_s N_C}{\pi}\log\frac{\mathbf{q}_j^2}{\lambda^2},\end{aligned} \tag{2.20}$$

which should only be evaluated for $\mathbf{p}_i^2 > \lambda^2$, and a simple phase-space slicing would then have been sufficient to organise the cancellation of divergences. However, while eq. (2.17) does describe the divergence in the soft limit, it is not an exact identity. We can account for the finite difference by including an integration over

$$\frac{-1}{t_it_{i+1}}V^\mu(q_i,q_{i+1})V_\mu(q_i,q_{i+1}) - \frac{4}{\mathbf{p}_i^2} \tag{2.21}$$

for $\mathbf{p}_i^2 < \lambda^2$. Numerically, it turns out to be sufficient to account for the difference and include this integral for values of $|\mathbf{p}_i|$ above roughly 0.2 GeV. The regulated matrix elements

JHEP06(2011)010

for *HEJ* are then given by

$$\begin{aligned}
\overline{\left|\mathcal{M}^{\text{reg}}_{\text{HEJ}}(\{p_i\})\right|}^2 = & \frac{1}{4\ (N_C^2-1)}\ \|S_{f_1f_2\to f_1f_2}\|^2 \\
& \cdot \left(g^2\ K_{f_1}\ \frac{1}{t_1}\right) \cdot \left(g^2\ K_{f_2}\ \frac{1}{t_{n-1}}\right) \\
& \cdot \prod_{i=1}^{n-2} \left(g^2 C_A \left(\frac{-1}{t_i t_{i+1}} V^\mu(q_i,q_{i+1}) V_\mu(q_i,q_{i+1}) - \frac{4}{\mathbf{p}_i^2}\ \theta\left(\mathbf{p}_i^2<\lambda^2\right)\right)\right) \\
& \cdot \prod_{j=1}^{n-1} \exp\left[\omega^0(q_j,\lambda)(y_{j-1}-y_j)\right], \\
\omega^0(q_j,\lambda) = & -\frac{\alpha_s N_C}{\pi} \log\frac{\mathbf{q}_j^2}{\lambda^2}.
\end{aligned} \tag{2.22}$$

Since the t-channel factorised matrix elements are very fast to evaluate and the regularisation procedure does not add any complexity (because of the simple IR structure of the t-channel factorised matrix elements), the radiative corrections to all orders can be constructed as an explicit phase space integral over each number of gluons emitted:[3]

$$\begin{aligned}
\sigma_{qQ\to 2j} = & \sum_{n=2}^{\infty} \prod_{i=1}^{n} \left(\int_{p_{i\perp}=0}^{p_{i\perp}=\infty} \frac{\mathrm{d}^2\mathbf{p}_{i\perp}}{(2\pi)^3} \int \frac{\mathrm{d}y_i}{2}\right) \frac{\overline{\left|\mathcal{M}^{\text{reg}}_{\text{HEJ}}(\{p_i\})\right|}^2}{\hat{s}^2} \\
& \times\ x_a f_{A,q}(x_a,Q_a)\ x_2 f_{B,Q}(x_b,Q_b)\ (2\pi)^4\ \delta^2\left(\sum_{k=1}^{n}\mathbf{p}_{k\perp}\right)\ \mathcal{O}_{2j}(\{p_i\}).
\end{aligned} \tag{2.23}$$

The cancellation of the poles in ε ensures that the logarithmic dependence on λ generated by the effective lower limit on the transverse momentum integrals cancels with the logarithmic λ-dependence of the virtual + unresolved-real correction, which generates the exponential factors of eq. (2.19). This is similar to the explicit construction of the solution to the BFKL evolution, where the very weak dependence of the solution on λ at leading logarithmic accuracy was studied in ref. [28, 29], and in ref. [19] at next-to-leading logarithmic accuracy. In appendix B we investigate the stability under variations in λ of a few of the cross-sections and distributions discussed throughout this paper. We find that the residual λ-dependence is very weak — see section B for further details. We then generally choose to use $\lambda = 0.5\,\text{GeV}$. Note that these findings are in good agreement with the conclusions from the studies of the λ-dependence of the explicit solutions to the BFKL equations [19, 28, 29, 41], where the convergence of the phase space integration could be checked explicitly against an analytic solution.

The only remaining unregulated divergences of $\overline{|\mathcal{M}^{\text{reg}}_{\text{HEJ}}|}^2$ are related to the region of zero transverse momenta of the partons extremal in rapidity.[4] A similar situation was discussed in ref. [21], where simply a cut on the transverse momentum of the extremal partons was introduced, and the dependence of the cross section on this cut studied. We have refined the

[3] The lower limit on the transverse momentum in the phase space integrals is understood to be small, but non-zero, so eq. (2.21) can still be evaluated numerically.

[4] Actually, with the emission vertex of eq. (2.10) there is also a collinear divergence for emissions close to the extremal partons from parts symmetrising $p_A \leftrightarrow p_1$ and $p_B \leftrightarrow p_n$. We avoid this divergence by not averaging over the two contributions for emissions which are clustered into the same jets as the extremal partons.

JHEP06(2011)010

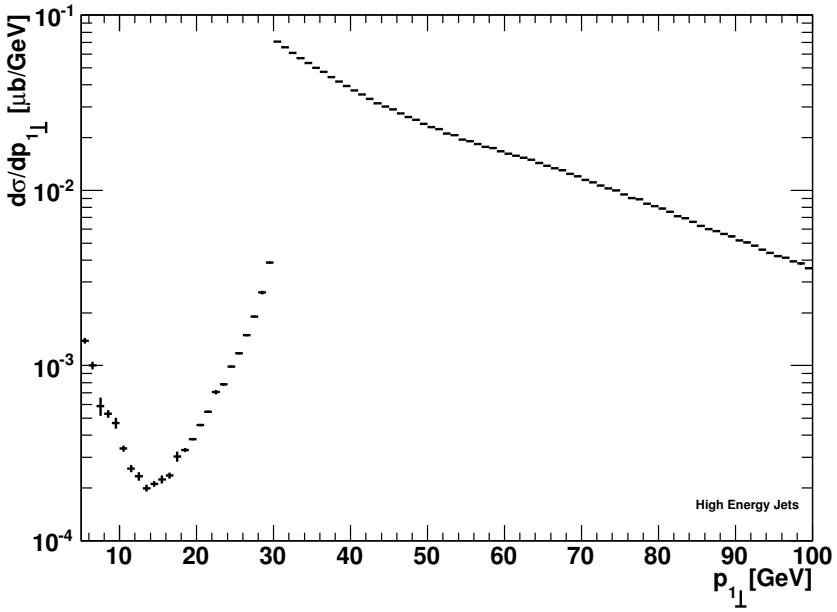

Figure 2. The dependence of the dijet cross section on the transverse momentum of the parton of lowest or highest rapidity. The step at 30 GeV is caused by the requirement of minimum 30 GeV transverse momentum by the hard jets.

treatment for the current study. If there is no hard jet associated with the extremal partons, they could be viewed as not participating in the proper hard scattering of the event. In the parton shower picture, such emissions would be counted as (in this case) initial state radiation, and the divergence regulated by the Sudakov form factors. The treatment of these are beyond the scope of the current paper, and we will simply require that the extremal partons are associated with (i.e. a member of) a hard jet. With this requirement, the dependence on a lower cut-off of the momentum allowed for the extremal partons is weak. This is illustrated in figure 2 for a dijet-sample at the 7 TeV LHC, requiring just[5] two anti-kt-jets with absolute rapidities less than 4.5, and with transverse momenta above 30 GeV. We see that the contribution from transverse momenta much smaller than the jet scale is small. The requirement that the extremal partons be associated with a hard jet has to a large extent regulated the divergence for vanishing transverse momentum of the extremal partons (compare with figure 16 of ref. [21]). In the results discussed in section 5, we will choose a lower limit on the transverse momentum of the extremal partons, which is 5 GeV smaller than the minimum transverse momentum required on hard jets. Removing the very small contribution from smaller scales simply improves the phase space integration. Furthermore, the unregulated divergence at zero transverse momentum has to be explicitly removed.

[5]Note that such a simple cut is problematic for NLO studies, because the truncation of the perturbative series introduces a large logarithmic dependence on any difference in the value of the cut applied on the two jets [42].

JHEP06(2011)010

The construction of an explicit integration over emissions to all orders relies on an efficient phase-space generator [20, 21], which should sample final states with the number of particles varying by more than an order of magnitude. The problem is significantly different to that of a so-called general purpose Monte Carlo (Pythia [43], Herwig [44], SHERPA [45]), since in these approaches, the approximation to the virtual corrections is *defined* such that the emission of particles is *unitary*, i.e. does not change the total cross section, which allows for a simple probabilistic interpretation. In *HEJ*, an approximation to the virtual corrections is calculated, and introduces a *suppression* of the regularised matrix element for any final state with a finite number of partons, as the rapidity length of the event is increased. This is countered by the (positive) contribution from the emission of additional gluons, and introduces a correlation between the number of final state partons and the typical rapidity length of an event. It is absolutely crucial to incorporate this probabilistic correlation in the phase space generator in order to obtain satisfactory numerical stability in a finite amount of time. Such a phase space integrator can be efficiently implemented by following the ideas of ref. [40]. The fully exclusive formulation in a flexible Monte Carlo facilitates the study of any observable.

3 Matching

The previous sections have set up the all-order approximations to jet production of *High Energy Jets*, and discussed the implementation as a flexible Monte Carlo, integrating explicitly over n-particle phase space. The resummation procedure generates only certain partonic phase space configurations (*FKL*-configurations, see section 2.2.1). The dijet production process is calculated within this approximation as (for notational brevity, we have omitted the label indicating the use of the regularised amplitudes)

$$\begin{aligned}\sigma_{2j}^{\text{resum}} = \sum_{f_1,f_2}\sum_{n=2}^{\infty}\prod_{i=1}^{n}\left(\int_{p_{i\perp}=0}^{p_{i\perp}=\infty}\frac{\mathrm{d}^2\mathbf{p}_{i\perp}}{(2\pi)^3}\int\frac{\mathrm{d}y_i}{2}\right)\frac{\overline{\left|\mathcal{M}_{\text{HEJ}}^{f_1f_2\to f_1g\cdots gf_2}(\{p_i\})\right|}^2}{\hat{s}^2}\\ \times\quad x_a f_{A,f_1}(x_a,Q_a)\; x_2 f_{B,f_2}(x_b,Q_b)\;(2\pi)^4\;\delta^2\left(\sum_{k=1}^{n}\mathbf{p}_{k\perp}\right)\;\mathcal{O}_{2j}(\{p_i\}),\end{aligned} \tag{3.1}$$

where the first sum is over the flavours f_1, f_2 of incoming partons. The distribution of any observable can be obtained by simply binning the cross section in eq. (3.1) in the appropriate variable formed from the explicit momenta. Obviously, multi-jet rates can also be calculated by multiplying by further multi-jet observables $\mathcal{O}_{3j}, \mathcal{O}_{4j}, \ldots$ in eq. (3.1).

In section 3.1 we will discuss how the amplitudes for the FKL-states included in eq. (3.1) can be corrected to full tree-level accuracy, limited only by the availability of full tree-level matrix elements. In section 3.2 we will discuss the inclusion of all remaining partonic configurations (in practice for up to 4 jets).

3.1 Matching for FKL configurations

Firstly, we want to match the description of the FKL n-jet configurations to the full tree-level matrix elements and thus improve upon the approximations inherent to the resummation. This can be straightforwardly done because of the flexibility inherent in eq. (3.1).

JHEP06(2011)010

Let $\mathcal{O}^e_{nj}(\{p_i\})$ denote the measurement function for *exclusive* n-jet production acting on the partonic phase space. This function will return one if the chosen jet-algorithm finds exactly n hard jets in the m-partonic phase space point, and returns zero otherwise. Furthermore, it will give access to the momenta of the n jets, $\{p_{\mathcal{J}_l}(\{p_i\})\}$. We note that $\mathcal{O}_{2j}(\{p_i\}) = \sum_{n=2}^{\infty} \mathcal{O}^e_{nj}(\{p_i\})$. In principle, we would then want to simply multiply each exclusive jet measure function with

$$\frac{\overline{|\mathcal{M}^{f_1 f_2 \to f_1 g \cdots g f_2}(\{p_{\mathcal{J}_l}(\{p_i\})\})|}^2}{\overline{|\mathcal{M}^{t, f_1 f_2 \to f_1 g \cdots g f_2}(\{p_{\mathcal{J}_l}(\{p_i\})\})|}^2}, \tag{3.2}$$

where the numerator is simply the (spin and colour summed and averaged) square of the full n-jet tree-level matrix element, and the denominator is the *HEJ*-approximation to this tree-level. This would ensure tree-level accuracy of the n-jet rates, while simultaneously weighing the n-jet samples with the virtual corrections from *HEJ*.

However, a few modifications to this naïve approach are necessary. Firstly, the jet momenta may not be of zero invariant mass. Secondly, the transverse momenta of the jets generally will not sum to zero, since some of the partons generated in the event may not be included in the hard jets. We therefore have to construct a new set of n jet-momenta to be used in the matching. We start by making each jet momentum equal to the sum of the parton momenta of each jet (each jet contains mostly just one hard parton after the *HEJ*-resummation). We then redistribute the transverse momenta of any partons not belonging to a jet among the hard jets, and remove these softer partons from the list of particles (and momenta) used in the matching. We choose to distribute the momenta in proportion to the transverse momenta of the resolved jets. If the sum of the momenta of the non-jet partons is q and the scalar sum of the transverse momenta of the jets is $P_\perp$, the new set of hard momenta $p^{\text{new}}_{\mathcal{J}_l}$ is given by

$$p^{\text{new}}_{\mathcal{J}_l} = p_{\mathcal{J}_l} + q * \frac{|p_{\mathcal{J}_{l\perp}}|}{P_\perp}. \tag{3.3}$$

The energy component of each jet is then finally reset to put it on-shell, and the momenta of the incoming partons are defined by energy/momentum conservation.

This reshuffling of momenta is illustrated for a sample event in figure 3, which has eleven partons in the final state, in a momentum configuration leading to four hard jets with transverse momentum above 30 GeV, found with the anti-kt jet algorithm, as implemented in FastJet [39]. The red circles show the positions in rapidity-phi space of the partons; the radii of the circles are proportional to the transverse energy of each parton and jet (and do not, therefore, represent the area of each jet). The green circles indicate the jets of the original event. As expected, they coincide with the hardest quarks/gluons. The blue circles indicate the reshuffled momenta used in the matching. Note, this procedure does not change the kinematics of the actual event; only the reweighing of the event to full tree-level accuracy is performed with matrix elements evaluated for the slightly modified momenta. If the threshold on the transverse momenta of jets was set very low, and the jets were finely resolved (small R-parameter), then no reshuffling of momenta would be

JHEP06(2011)010

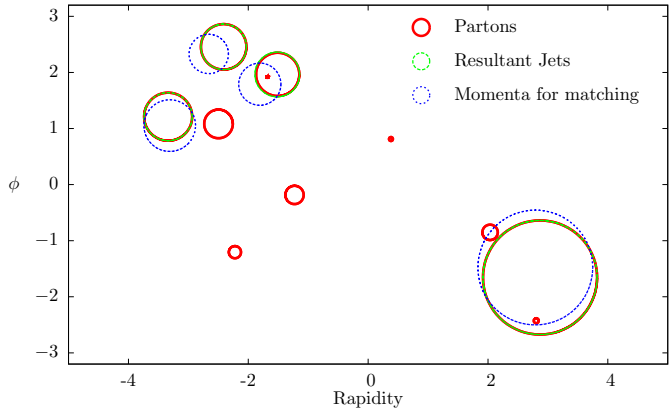

Figure 3. This plot shows for an example event the momenta of the partons (red), the resultant jets from FastJet (green) and the reshuffled momenta described in the text (blue). The radii of the circles are proportional to the transverse momentum of the particle or jet described.

necessary. However, the full matrix elements can only be evaluated for states of relatively low multiplicity (with MadGraph [46], we limit ourselves to matching of up to four jets). So with a low jet matching scale, the available fixed order matrix elements for matching would cover only a small part of the total cross section. A similar issue occurs for the CKKW-L [6, 7] or MLM [8] style matching of parton shower algorithms.

We then reweigh each event generated with the following multiplicative matching factor, evaluated with the on-shell hard momenta as found by the described procedure:

$$w_{n-\text{jet}} \equiv \frac{\overline{\left|\mathcal{M}^{f_1 f_2 \to f_1 g \cdots g f_2}\left(\left\{p^{\text{new}}_{\mathcal{J}_l}(\{p_i\})\right\}\right)\right|^2}}{\overline{\left|\mathcal{M}^{t,f_1 f_2 \to f_1 g \cdots g f_2}\left(\left\{p^{\text{new}}_{\mathcal{J}_l}(\{p_i\})\right\}\right)\right|^2}}. \tag{3.4}$$

In this notation, we have suppressed the flavour and momentum-dependence of w_n, but it is obviously calculated on an event-by-event basis. The FKL-matched cross section is then found as

$$\begin{aligned}\sigma^{\text{resum,match}}_{2j} = &\sum_{f_1,f_2}\sum_{n=2}^{\infty}\prod_{i=1}^{n}\left(\int_{p_{i\perp}=\lambda}^{p_{i\perp}=\infty}\frac{\mathrm{d}^2\mathbf{p}_{i\perp}}{(2\pi)^3}\int\frac{\mathrm{d}y_i}{2}\right)\frac{\overline{|\mathcal{M}^{f_1 f_2\to f_1 g\cdots g f_2}_{\text{HEJ}}(\{p_i\})|}^2}{\hat{s}^2}\\ &\times\sum_m \mathcal{O}^e_{mj}(\{p_i\})\; w_{m-\text{jet}}\\ &\times\; x_a f_{A,f_1}(x_a,Q_a)\; x_2 f_{B,f_2}(x_b,Q_b)\;(2\pi)^4\;\delta^2\left(\sum_{i=1}^{n}\mathbf{p}_{i\perp}\right)\;\mathcal{O}_{2j}(\{p_i\}).\end{aligned} \tag{3.5}$$

The impact of this matching procedure can be seen in figure 4, which displays the differential dijet cross section wrt. the rapidity difference Δy_{fb} between the most forward/backward hard jet, within the following set of cuts:

$$p_{j_\perp} > 60\,\text{GeV} \quad |y_j| < 4.5 \quad \text{anti}-\text{kt}, R = 0.6. \tag{3.6}$$

JHEP06(2011)010

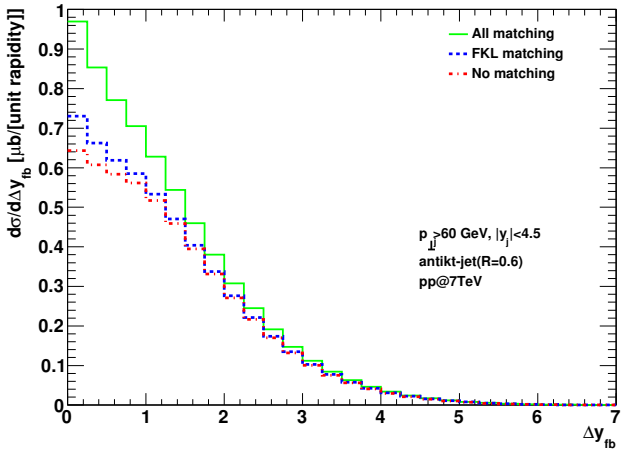

Figure 4. This plot shows the impact of matching in jet production, as a function of rapidity span. The initial HEJ approximation is shown (red, dot-dashed) together with matching to FKL configurations (blue, dashed) and matching to both FKL and non-FKL configurations (green, solid).

The matching scale is set equal to the general jet scale of 60 GeV. The red (dot-dashed) curve is the result of the pure resummation; the blue (dashed) curve is obtained after matching of the states arising in the resummation up to four hard jets. The correction is small throughout, being slightly more significant at low rapidity spans.

3.2 Matching for non-FKL configurations

The processes and partonic configurations which do not arise in the resummation are included straightforwardly by adding these to the dijet rate found by the (matched) eq. (3.1). For example, we can add the remaining contribution to the exclusive dijet rate as

$$\sigma_{2j}^{\text{non-FKL}} = \sum_{f_1,f_2}\sum_{f_{f1},f_{f2}}\prod_{i=1}^{2}\left(\int_{p_{i\perp}=p_{\perp\min}}^{p_{i\perp}=\infty}\frac{\mathrm{d}^2\mathbf{p}_{i\perp}}{(2\pi)^3}\int\frac{\mathrm{d}y_i}{2}\right)\frac{\overline{|\mathcal{M}^{f_1f_2\to f_{f1}f_{f2}}(\{p_i\})|}^2}{\hat{s}^2} \tag{3.7}$$
$$\times\,\Theta(\{f_i\},\{p_i\})\;x_a f_{A,f_1}(x_a,Q_a)\;x_2 f_{B,f_2}(x_b,Q_b)\;(2\pi)^4\;\delta^2\left(\sum_{i=1}^{n}\mathbf{p}_{i\perp}\right)\;\mathcal{O}_{2j}(\{p_i\}),$$

where $p_{\perp\min}$ is the minimum transverse momentum required for hard jets. The function $\Theta(\{f_i\},\{p_i\})$ returns one if the parton and momentum configuration is of non-FKL status. If only rapidity ordered sets of momenta p_i are generated, then one needs to also sum (or Monte Carlo sample) over all possible assignments between momenta and the particles in the process. The generalisation to the three and four jet states is straightforward, and the final result for the dijet rate is

$$\sigma_{2j} = \sigma_{2j}^{\text{resum,match}} + \sum_n \sigma_{nj}^{\text{non-FKL}}. \tag{3.8}$$

Each component is implemented by explicit Monte Carlo sampling over phase space and an evaluation of matrix elements. Therefore, any observable can be constructed and studied, also after matching has been included in the formalism.

JHEP06(2011)010

The impact of the non-FKL states is indicated on figure 4, where the green (solid) line is obtained from the sum of all terms in eq. (3.8). This correction is again more significant for small rapidity spans, as we expect.

4 Logarithmic corrections to the scale choice

The discussions so far have made no assumptions on the scale choice made for the evaluation of α_s or the pdfs. In this section we will compare the results arising for a fixed scale choice (of e.g. the minimum jet transverse momentum), and a scale choice made event by event equal to the maximum jet transverse momentum of the event. Finally, we will include pieces of the next-to-leading logarithmic corrections to the BFKL kernel, which will stabilise the dependence on the scale choice. This will then form the basis of the standard scale choice for the results presented in section 5.

The connection between the formalism of *High Energy Jets* and that of BFKL [14–16, 33, 47] is that in the limit of large invariant mass between all partons (conditions relaxed for neighbouring pairs of particles at NLL [48]), then the amplitudes underlying the BFKL formalism coincide with those of *HEJ* (and with those of full QCD). The NLL corrections to the BFKL kernel have two origins: the one-loop corrections to one-gluon emission, and the contribution from two-gluon and quark-anti-quark-emission in quasi-multi-Regge-kinematics (i.e. not necessarily a large invariant mass between the pair of particles). The net result of the corrections is a sum of an expression with the same functional form as the LL kernel, multiplied by a running coupling logarithm, and a term of a more complicated kinematic structure [18, 19]. The relevant discussion of the regularisation of the NLL corrections to the BFKL kernel was presented in ref. [18, 19, 41]. We repeat it here, with a notation tailored to the present application.

The NLL BFKL kernel is expressed in terms of a transverse momentum, which is the transverse momentum of the emitted gluon, or the sum of transverse momenta of the emitted pair of gluons or quark-anti-quark pair. All other kinematic dependence is integrated over before arriving at the BFKL kernel. In $D = 4 + 2\varepsilon$ the BFKL amplitudes obey the following relation at NLL accuracy (compare with eq. (2.17))

$$\overline{\left|\mathcal{M}^{\text{BFKL}}_{p_a\ p_b\to p_1\ \cdots\ p_{i-1}\ p_i\ p_{i+1}\ \cdots\ p_n}\right|^2} = \mathcal{K}^r(\mathbf{p}_i)\ \overline{\left|\mathcal{M}^{\text{BFKL}}_{p_a\ p_b\ \to\ p_1\ \cdots\ p_{i-1}\ p_{i+1}\ \cdots\ p_n}\right|^2}, \tag{4.1}$$

with $\mathcal{K}^r(\mathbf{p}_i) = K^r_\varepsilon(\mathbf{p}_i) + K^r(\mathbf{p}_i)$, where $K^r(\mathbf{p}_i)$ is irrelevant for the current discussion, and

$$\begin{aligned} K^r_\varepsilon(\mathbf{p}_i) = \frac{4\ g_\mu^2\mu^{-2\varepsilon}\ C_A}{\mathbf{p}_i^2}\Bigg[1+\frac{g_\mu^2\mu^{-2\varepsilon}C_A\Gamma(1-\varepsilon)}{(4\pi)^{2+\varepsilon}}\Bigg(\beta_0/N_C\frac{1}{\varepsilon}\left\{1-\left(\frac{\mathbf{p}_i^2}{\mu^2}\right)^{\varepsilon}\left(1-\varepsilon^2\frac{\pi^2}{6}\right)\right\} \\ +\left(\frac{\mathbf{p}_i^2}{\mu^2}\right)^{\varepsilon}\left(\frac{4}{3}-\frac{\pi^2}{3}+\frac{5}{3}\frac{\beta_0}{N_C}\ +\ \varepsilon\left(14\zeta(3)-\frac{32}{9}-\frac{28}{9}\frac{\beta_0}{N_C}\right)\right)\Bigg)\Bigg], \end{aligned} \tag{4.2}$$

JHEP06(2011)010

with $\beta_0 = \frac{11}{3}N_C - \frac{2}{3}n_f$. The NLL-corrections to the trajectory give

$$\begin{aligned}\hat{\alpha}(q^2) = &-\bar{g}_\mu^2\,\frac{2}{\varepsilon}\,\left(q^2/\mu^2\right)^\varepsilon\left(1+\frac{\bar{g}_\mu^2}{\varepsilon}\left[(\beta_0/N_C)\left(1-\frac{\pi^2}{6}\varepsilon^2\right)\right.\right.\\ &-\left(\frac{q^2}{\mu^2}\right)^\varepsilon\left(\frac{11}{6}+\left(\frac{\pi^2}{6}-\frac{67}{18}\right)\varepsilon+\left(\frac{202}{27}-\frac{11\pi^2}{18}-\zeta(3)\right)\varepsilon^2\right.\\ &\left.\left.\left.-\frac{n_f}{3N_C}\left(1-\frac{5}{3}\varepsilon+\left(\frac{28}{9}-\frac{\pi^2}{3}\right)\varepsilon^2\right)\right)\right]\right).\end{aligned} \tag{4.3}$$

By applying the same regularisation procedure as discussed in section 2.4 we find that for both the real emission (evaluated above $\mathbf{p}_i^2 > \lambda^2$) and for the trajectory the term found at LL accuracy is multiplied by a running coupling logarithm. For the real emission this is:

$$\left(\frac{4\;g_\mu^2\;C_A}{\mathbf{p}_i^2}\right)\left(1-\frac{g_\mu^2}{(4\pi)}\frac{\beta_0}{4\pi}\ln\mathbf{p}_i^2/\mu^2\right). \tag{4.4}$$

For the regularised trajectory we find

$$\omega_0(q,\lambda) = \frac{\alpha_s\;C_A}{\pi}\ln\left(\frac{\lambda^2}{q^2}\right)\;\left(1+\frac{\alpha_s}{2}\frac{\beta_0}{4\pi}\ln\frac{\mu^4}{q^2\lambda^2}\right). \tag{4.5}$$

These results are in complete agreement with what was found in ref. [18, 19]. The logarithm of the trajectory may seem a little odd (being dependent on λ), but it reproduces the NLL BFKL results when expanded in β_0. Besides, the study of the pure NLL BFKL correction in ref. [18, 19, 49], show that the organisation of the cancellation of soft divergence is completely stable for the values explored for λ.

We finish off this section with a simple study illustrating the impact of various scale choices on the average number of hard jets versus the rapidity difference between the most forward/backward jet within the cuts of eq. (3.6). We apply three different choices: 1) a fixed scale choice of 60 GeV, 2) a common scale choice, chosen event by event, of the largest transverse momentum of any jet, and 3) the latter, including the logarithmic corrections discussed above.

This observable is just one of many with a strong correlation with the number of hard jets — in order to describe the region of phase space of large Δy_{fb}, it is clearly imperative to describe correctly the emissions of many hard jets. Other such examples are studied in the next section. The obvious expectation is that for a larger value of α_s (smaller scale), one would see more hard jets than for a smaller value of α_s (larger scale). Indeed, this is found in figure 5 for rapidity differences less than roughly 5. Furthermore, we see that including the logarithmic corrections outlined above leads to a prediction in-between that of the fixed, low scale choice of 60 GeV, and the choice of the hardest jet scale. This is of course entirely as expected. For larger rapidities, phase space constraints become increasingly important, and the scale at which the pdfs are evaluated will influence the details. Eventually, as Δy_{fb} increases further, the average number of hard jets decreases as the phase space for additional radiation is reduced when the energy of the forward/backward jets gets close to the total available hadronic energy.

JHEP06(2011)010

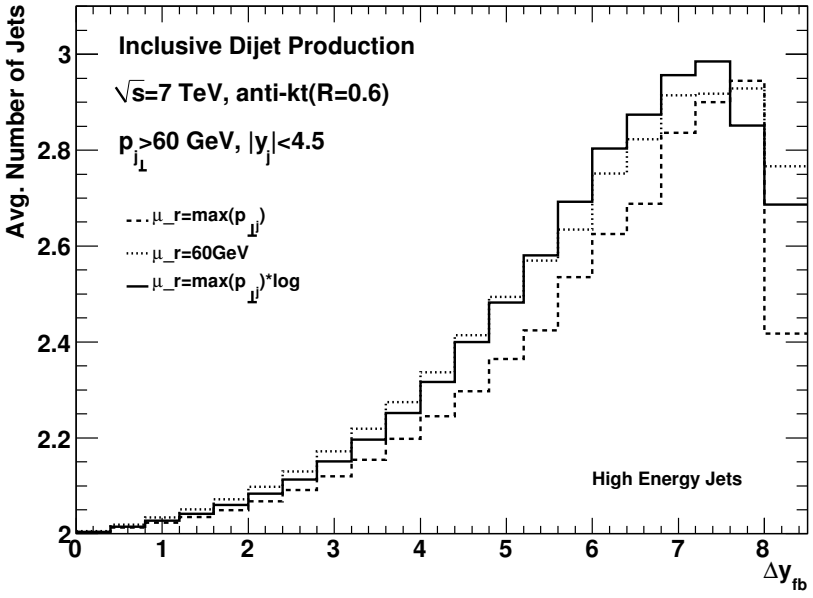

Figure 5. The average number of hard jets ($p_\perp > 60\,\mathrm{GeV}$) in inclusive dijet production as a function of the difference in rapidity Δy_{fb} between the most forward/backward hard jet.

5 Results

In this section we present results for dijet- and trijet-studies within these cuts (identical to those of eq. (3.6) in section 3.1):

$$p_{j_\perp} > 60\,\mathrm{GeV} \quad |y_j| < 4.5 \quad \mathrm{anti-kt}, R = 0.6. \tag{5.1}$$

We choose as the standard scale choice $\mu_r = \max_j(p_{\perp j})$, and include the running coupling logarithms from NLL accuracy, as discussed in section 4. As shown explicitly in appendix C, the all-order framework of *High Energy Jets* is free from the instability seen in the NLO-calculation of dijet production [42] when the transverse momentum cut on the two jets is equal. This problem simply arises from the fact that in a three-particle system, the cut on the transverse momentum of two particles automatically changes the phase space explored by the transverse momentum of the third particle. The infra-red region of the real emission corrections to the dijet system is explored in the limit where the two transverse momenta of the hard jets are equal. An off-set $\Delta p_\perp$ in the cut of the two hardest jets modifies the soft phase space for additional real emission, and can therefore introduce a logarithmic dependence on $\Delta p_\perp$. However, this dependence seems specific to cross sections terminated at NLO, and is washed away in several other all-order frameworks, e.g. POWHEG [10, 50, 51] (NLO matched to a parton shower) and the BFKL generator studied in ref. [30]. Since the problem is related to a fixed-order perturbative calculation rather than any observation or our description, we will proceed with an equal cut on the transverse momentum of all jets. Since the numerical estimate of the dijet cross section with equal cuts on the transverse

JHEP06(2011)010

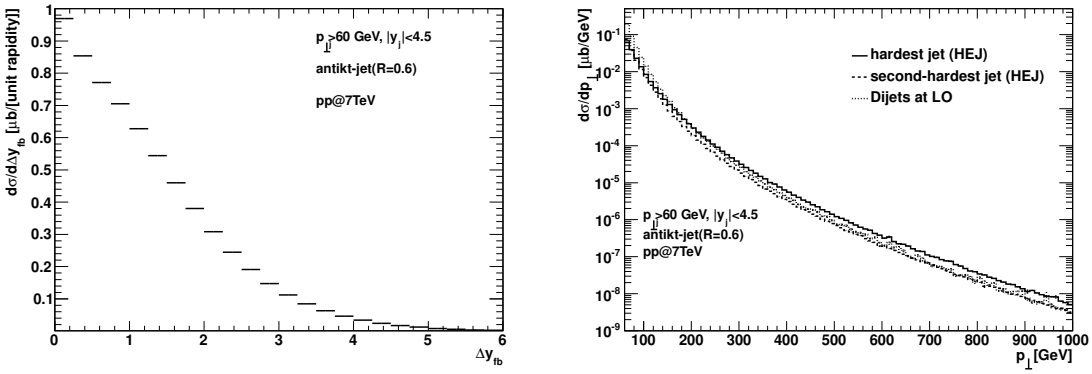

Figure 6. The differential dijet-rate with respect to the rapidity difference between the most forward and most backward hard jet (left) and the transverse momentum of the hardest and second-hardest jet of the event (right).

momenta differs significantly from LO to NLO, and again from NLO to NLO with a parton shower (like e.g. POWHEG [10, 50, 51]) it will be interesting to confront such data with the theoretical descriptions, including the one of *High Energy Jets*.

We will apply the anti-kt jet-clustering algorithm as defined and implemented in ref. [39] with $R = 0.6$. We define Δy_{fb} as the rapidity difference between the most forward and most backward hard jet. The average number of jets in the events is an obvious indication of the importance of the hard, higher order corrections that are resummed in *High Energy Jets*. In section 5.1.1 we study simple characteristics of the inclusive sample generated with *HEJ*; we then move on to discuss distributions in $p_\perp$, H_T (scalar sum of transverse momenta) and s_{ij} (invariant mass between hardest jets), where the corrections have a particularly large impact. Other all-order approaches like e.g. Cascade [52, 53] calculate higher order corrections in the k_t-factorisation scheme through the evolution of off-shell pdfs convoluted with a $2 \to 2$ (off-shell) hard scattering matrix element. It would be interesting to compare the predictions for these observables also from such a framework.

5.1 Dijet studies

5.1.1 Rapidity and transverse momentum distributions

In figure 6 we have plotted the differential cross section with respect to both Δy_{fb} (left) and the transverse momentum of the hardest and second-hardest jet in the event (right). The dijet rate is peaked at zero rapidity difference, and the radiative corrections have clearly induced a difference in the transverse momentum distribution of the hardest and second-hardest jet (which is obviously identical at leading order). The transverse momentum spectrum is compared to that arising in a LO calculation (using the MSTW2008LO pdf set, and setting the renormalisation and factorisation scale equal to $p_{\perp j}$). The LO spectrum is significantly softer then that of the hardest jet arising in *HEJ*.

JHEP06(2011)010

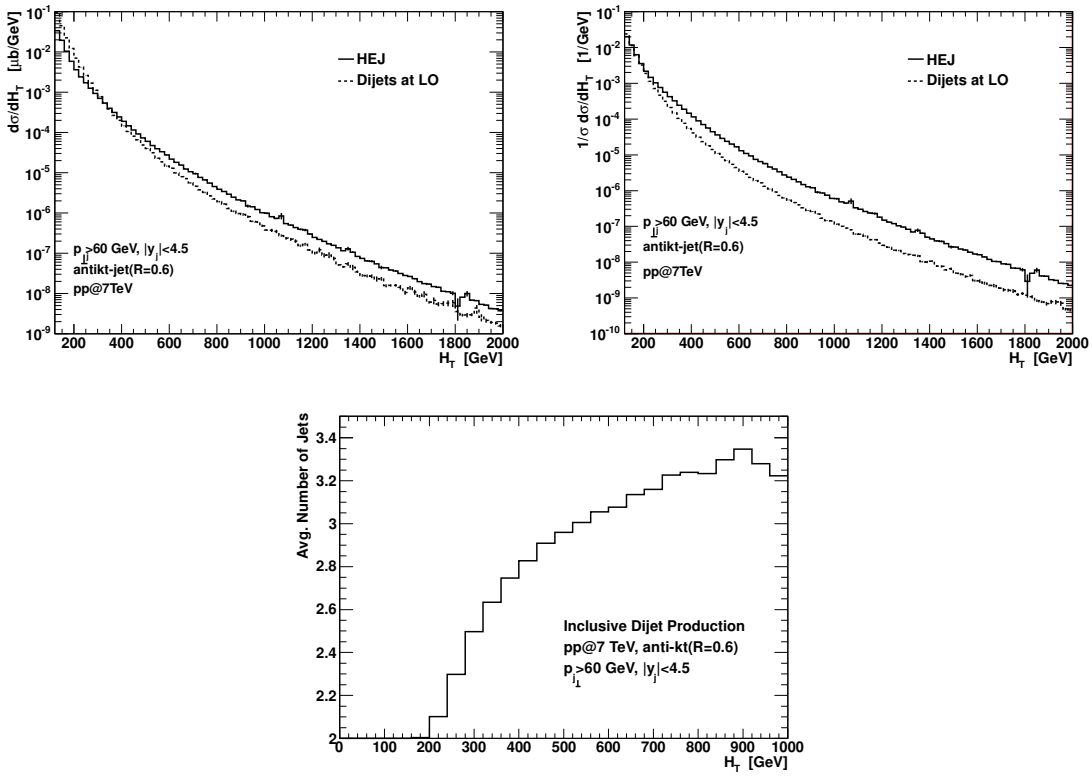

Figure 7. The differential cross section with respect to H_T (top left), and the normalised spectrum (top right). The radiative corrections implemented in *High Energy Jets* enhance the high-H_T-tail significantly. The bottom plot is of the average number of hard jets (transverse momentum above 60 GeV) in the events as a function of H_T. Hard radiative corrections, as those included in HEJ, are clearly important in the description of events with large H_T.

5.1.2 Δy_{fb}, H_T, $s_{j_1 j_2}$ and the average number of jets

In figure 5 we plotted the average number of hard jets (transverse momentum larger than 60 GeV) according to the anti-kt jet algorithm with $R = 0.6$ in the inclusive dijet sample, as a function of the rapidity span Δy_{fb} between the most forward and most backward hard jet. As expected, there is a strong correlation between Δy_{fb} and the average number of hard jets. The average number of hard jets rises monotonously until $\Delta y_{\text{fb}} \approx 7$, simply because the partonic phase space increases. However, as the rapidity span is increased further, the parton density functions fall off so steeply as $x \to 1$ that the production of additional hard jets beyond the required dijet system is effectively vetoed.

One observable which is often used in the search for signals of new physics at hadron colliders is the scalar sum of transverse energy (or momentum) in the hard event. For the jet studies, we define it as

$$H_T = \sum_j |p_{\perp j}|, \tag{5.2}$$

where the sum runs over the jets found with a given jet-algorithm, with a transverse mo-

JHEP06(2011)010

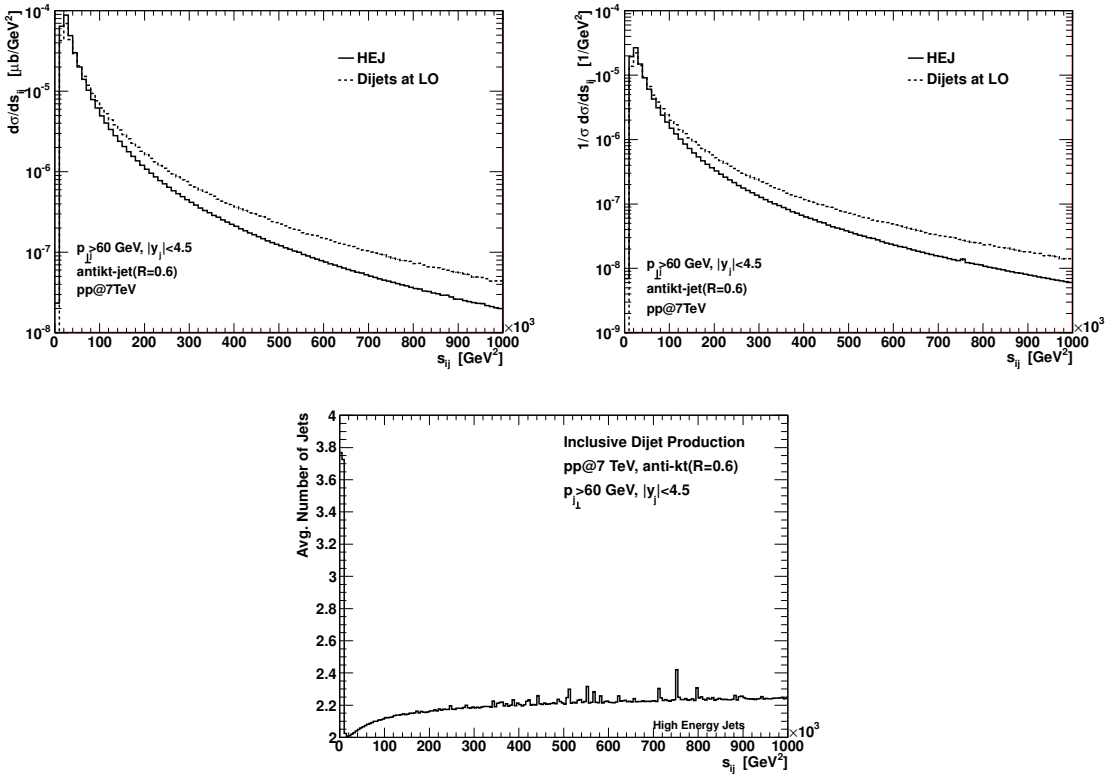

Figure 8. The differential cross section with respect to the square of the invariant mass s_{ij} between the two hardest jets (top left), and the normalised spectrum (top right). The bottom plot is of the average number of hard jets (transverse momentum above 60 GeV) in the events as a function of s_{ij}. Please see text for discussion.

mentum bigger than some hard cut-off. In figure 7 (top right) we plot the differential cross section wrt. H_T as obtained both at leading order QCD, and within *HEJ*. The distribution is clearly more pronounced at large H_T when the higher order corrections from *HEJ* are included. This is made very clear on the plots of the normalised H_T-distribution at the top right of figure 7. The bottom plot in figure 7 is of the average number of jets in the events as a function of H_T. We see that the average number of jets starts at 2, and very quickly rises above 3 (already at roughly 600 GeV). A priori, one might have expected the large-H_t tail to be dominated by two hard jets. Figure 7 clearly demonstrates this is not the case. Furthermore, the very high average number of jets in the large-H_T tail of the dijet distribution suggests that a veto on further hard jets beyond two would be very efficient in suppressing the QCD contribution to large-H_T dijet events. The rise in the number of hard jets is a direct consequence of the t-channel colour exchange, and therefore may be different between the QCD process and any process originating from new physics.

In figure 8 we plot the same three quantities for s_{ij}, the square of the invariant mass between the two *hardest* jets of the event. From the top-right plot of the normalised distribution we see that the corrections implemented in *HEJ* lead to a relative enhancement

JHEP06(2011)010

at small s_{ij}, and a suppression at large s_{ij} compared to the LO result. This behaviour can be explained by the fact that the radiative corrections implemented in *HEJ* will fill the rapidity span between the two LO jets, as seen in e.g. figure 5. The hardest jets are likely to be the ones that are radiated centrally in rapidity (a similar effect was seen in ref. [21]). For any value of the rapidity span Δy_{fb} between the most forward and most backward hard jet, the higher order corrections implemented in *HEJ* can produce a central jet, which has a slightly harder transverse momentum spectrum than the extremal ones, and is therefore more likely to be the one(s) used in the definition of s_{ij}. For all values of Δy_{fb}, the *HEJ*-corrections will lead to a smaller value Δy_h of the rapidity span between the two hardest jets in the event. This in turn induces a smaller value of s_{ij} than would be the case in the description of LO exclusive dijets.

The average number of jets versus s_{ij} is shown at the bottom of figure 8. At small values of s_{ij} it is peaked at almost 3.8, then falls off abruptly to 2 already at $s_{ij} = 2 \cdot 10^4 \text{GeV}^2$, and then rises to a plateau at 2.25. This behaviour is a sum of two effects. The events at small s_{ij} are dominated by the cases where two additional (central) jets have been radiated by the *HEJ*-mechanism; these two jets are often the hardest (in pt), and therefore define s_{ij} (which can be small since the jets can be aligned in $p_\perp$ (i.e. they do not have to be back-to-back in azimuth as dijets at LO) and close in rapidity). The strong peak at small s_{ij} is therefore an (at least) α_s^2-correction to the tree-level dijets. There is another effect, giving rise to a distribution increasing with s_{ij}, starting at 2 for $s_{ij} = 0$ and then reaching the plateau. This is just the standard $\mathcal{O}(\alpha_s)$-effect of one hard radiation. The value 2.25 is not too far from the value for the average number of jets in the fully inclusive dijet sample generated with *HEJ*, so the plateau is just an indication of only a small correlation between s_{ij} and the average number of jets. However, for the $\mathcal{O}(\alpha_s)$-correction of additional jets to arise and the average number of jets to rise from the LO value of two, a rapidity difference between the two jets is required (c.f. figure 5), and this naturally leads to an increase in $\hat{s}_{ij}$. This is why the average number of jets is close to 2 only for small $\hat{s}_{ij}$.

While the integral of the curves for $\mathrm{d}\sigma/\mathrm{d}H_T$ and $\mathrm{d}\sigma/\mathrm{d}s_{ij}$ are equal to the total cross section, the same neither is nor should be the case for the average number of jets vs. $\mathrm{d}\sigma/\mathrm{d}H_T$ and $\mathrm{d}\sigma/\mathrm{d}s_{ij}$. Here, instead the integrals $\int \mathrm{d}\sigma/\mathrm{d}H_T$ AvgJets(H_t) $\mathrm{d}H_T$ and $\int \mathrm{d}\sigma/\mathrm{d}s_{ij}$ AvgJets(s_{ij}) $\mathrm{d}s_{ij}$ should equal the average number of jets in the inclusive dijet sample. As shown in figures 7 and 8, $\mathrm{d}\sigma/\mathrm{d}H_T$ spans 7 orders of magnitude whereas $\mathrm{d}\sigma/\mathrm{d}s_{ij}$ spans only about 4. Therefore, the average number of jets can rise very high in the tail of the H_T-distribution, and still have little impact on the average number of jets in the inclusive dijet sample. However, the large-H_T-tail is of course of particular interest in BSM searches.

5.2 Trijet studies

In this section we will briefly present the distributions discussed previously, but this time for events with at least three hard jets. Many of the features identified in inclusive dijet production, like e.g. the strong correlation between the average number of jets and the rapidity difference between the most forward and most backward hard jet are found also for 3-jet production.

JHEP06(2011)010

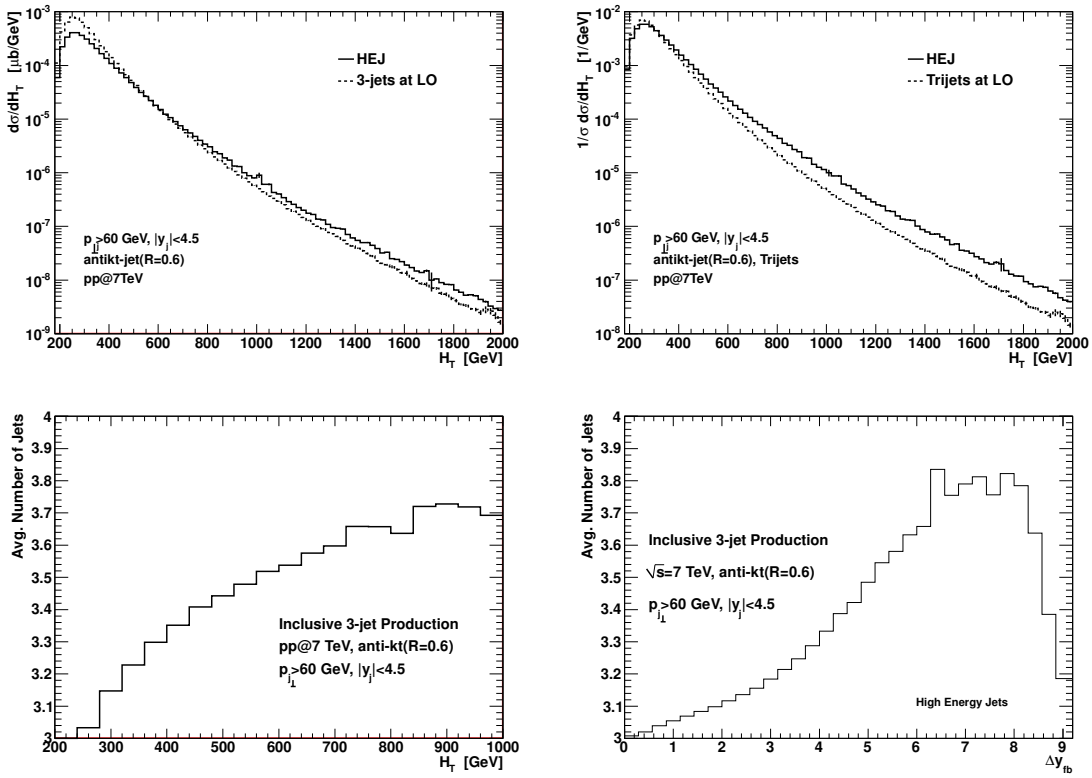

Figure 9. The differential 3-jet cross section with respect to H_T (top left), and the normalised spectrum (top right). The radiative corrections implemented in *High Energy Jets* enhance the high-H_T-tail significantly. The bottom plot is of the average number of hard jets (transverse momentum above 60 GeV) in the events as a function of H_T. Hard radiative corrections, as those included in HEJ, are clearly important in the description of events with large H_T.

On the top of figure 9 we compare the results for the H_T-distribution in 3-jet production as obtained in leading order and in *High Energy Jets*. Top left is the distribution in absolute numbers, on the top right the distribution is divided by the total 3-jet cross section. Just as in the dijet case, the higher order corrections implemented in HEJ hardens the spectrum in H_T. The average number of hard jets vs. H_T is shown on the lower left of figure 9. The distribution rises to 3.6 at $H_T = 800\,\text{GeV}$ and then drops off slightly for increasing H_T. We note that the in the trijet case, the average number of jets rises 0.6 units above the minimum required, whereas in the dijet case it rises a full 1.2 units. Both cases represent of course large corrections to the simplistic tree-level point of view. The lower right plot on figure 9 is of the average number of jets vs. the rapidity span between the most forward/backward hard jets. It rises from 3 to roughly 3.8 at rapidity differences between 7 and 8, before dropping back down towards 3, again because the increase in x necessary for additional radiation leads to a pdf suppression. An increase in the centre-of-mass energy of the proton-proton collision will obviously lead to a further increase in the number of hard jets produced.

In figure 10 we study the distributions in the invariant mass between the two hardest jets in the event. Similarly to the dijet-case, we find that the results from *HEJ* are sup-

JHEP06(2011)010

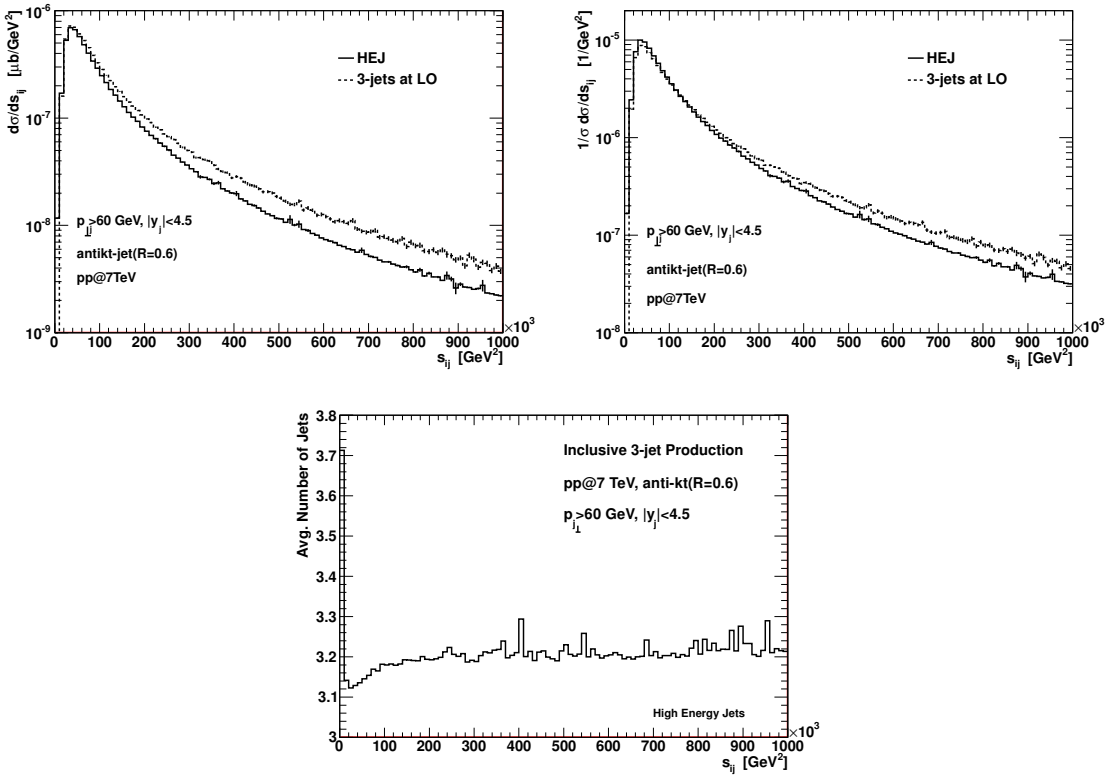

Figure 10. The differential 3-jet cross section with respect to the square of the invariant mass s_{ij} between the two hardest jets (top left), and the normalised spectrum (top right). The bottom plot is of the average number of hard jets (transverse momentum above 60 GeV) in the events as a function of s_{ij}. Please see text for discussion.

pressed at large s_{ij} compared to the 3-jet LO estimate. The bottom plot on figure 10 is of the average number of jets in inclusive 3-jet events as a function of the invariant mass between the two hardest jets. The distribution is very strongly peaked at small s_{ij} for exactly the same reason as the dijet case: the correction from additional jet production allows for two central (and thus generally slightly harder in transverse momentum) jets, which can form a system of small invariant mass. In fact, the average number of jets in inclusive 3-jet production at small s_{ij} is almost identical to the average number of jets in inclusive dijet production at small s_{ij}.

5.3 Gaps between di-jets

It is possible to construct several observables which are sensitive to additional radiation from the dijet-system, and thus can be used as a direct test of the description arrived at using various descriptions like e.g. fixed order [54–59], shower, Cascade [52, 53], analytic approaches [60, 61] and *HEJ*. There is a small challenge in defining quantities which are stable within each perturbative framework. We have already discussed that the NLO calculation for dijet production is unstable in a setup of equal transverse momentum cuts on the two jets [30, 42], but that it can be stabilised by requiring e.g. cuts of 65 GeV

JHEP06(2011)010

and 60 GeV on the hardest and next-to-hardest jet. Some dijet observables will then be calculable in several frameworks. A well-studied example of an "inclusive" dijet observable is the average of $\cos(\pi - \phi_{jj})$ vs. Δy_{fb}. At LO, the two jets are obviously back-to-back, and $\cos(\pi - \phi_{jj}) = 1$. The benefit of this observable is that it is completely inclusive in the radiation between the two jets (this inclusiveness allows for studies also within (semi-)analytic approaches of BFKL [62, 63]) - any emission will cause a decorrelation, whether or not it is identified as a separate jet. An experimental study of this quantity could serve as a strong test of the description of higher order corrections.

Instead of studying the effect of additional radiation through its impact on the jets extremal in rapidity, one can study the radiation in-between the dijets directly. The Atlas collaboration have published a note on such a study in early data from the LHC [64]. They present data for the so-called "gap fraction", defined as the fraction of dijet events with no additional hard jets between the two (in rapidity). We have already seen (e.g. figure 5) that the average number of hard jets in dijet events increases with the rapidity difference between the forward/backward jet, and this should obviously be reflected in the "gap fraction". These early studies also serve to guide jet veto studies for Higgs boson production in association with dijets [3, 65]. For these studies, it is of interest to use a small transverse scale for the vetoing of further jets. The Atlas study defined jets using the anti-k_t algorithm, with $R = 0.6$, and a transverse scale of 30 GeV. In order to ensure a sufficiently small dijet-rate (and thus an acceptable scaling factor for the trigger), a harder scale was required. We will here concentrate on the part of the study, where the average transverse momentum of the two jets extremal in rapidity was required to be above 60 GeV. The cuts used are then:

$$p_{j_\perp} > 30\,\text{GeV} \quad \bar{p}_\perp > 60\,\text{GeV} \quad |y_j| < 4.5 \quad \text{anti} - \text{kt}, R = 0.6. \tag{5.3}$$

where $\bar{p}_\perp$ is the average transverse momentum of the most forward/backward jets.

Figure 11 presents the prediction for both the average number of hard jets (with a transverse momentum larger than 30 GeV) and the gap fraction obtained using *HEJ*, within the cuts in eq. (5.3). We have also indicated the variation in both quantities between a scale choice of 30 GeV, $\max(p_{\perp j})$ and of $\max(p_{\perp j})$ including the logarithmic corrections discussed in section 4, all using the pdfs included in MSTW2008 [66]. For the last, "central" scale choice we also present the results obtained by using NNPDF2.0 [67], including the full envelope of the 100 uncertainty pdfs. The uncertainty induced by the pdfs on these quantities is completely negligible (they begin to play a role at $\Delta y_{\text{fb}} > 8$). The uncertainty estimate induced by a variation in the renormalisation and factorisation scale between 30 GeV (the minimum transverse scale for jets) and $\max(p_{\perp j})$ is increasing for increasing rapidity spans, and amounts to a variation between 3.6 and 4.0 in the average number of jets (with a transverse momentum larger than 30 GeV) for a rapidity span of 7. These results are marked by the outer solid lines (on both plots). The central solid line is obtained by choosing the renormalisation scale $\max(p_{\perp j})$, but including the logarithms as discussed in section 4. The results obtained by choosing the renormalisation scale as 30 GeV and including the logarithms is almost identical.

The pdf and scale uncertainty of the predictions for the average number of jets and the gap fraction are sufficiently small that the the ideas and calculations presented here can be meaningfully confronted with data, once it has become available.

JHEP06(2011)010

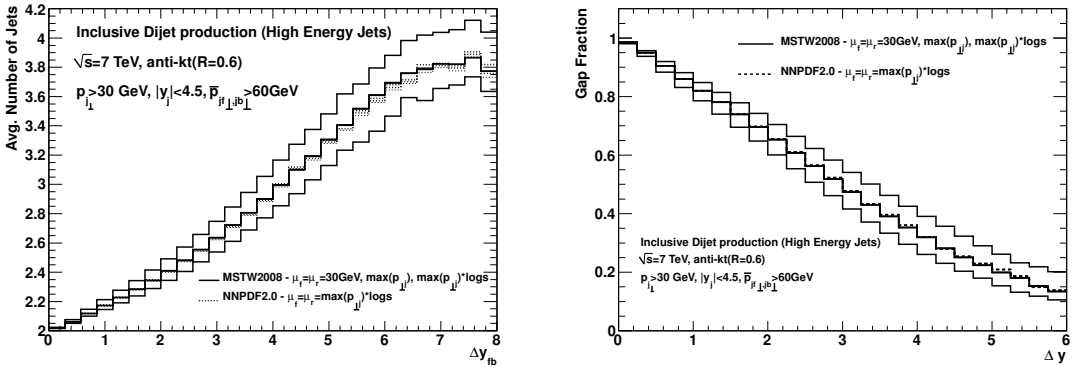

Figure 11. The average number of jets and gap fraction vs. the rapidity difference Δy_{fb} between the most forward and most backward jets. The upper and lower solid lines are for scale choices of 30 GeV and $\max(p_{\perp j})$ respectively. The central solid lines are for a scale choice of $\max(p_{\perp j})$ plus the logarithms of section 4 for MSTW2008 [66] uncertainty pdf sets. The difference between the sets is barely observable. Also shown in dotted and dashed lines are the results with the uncertainty sets from NNPDF2.0 [67].

6 Summary and conclusions

We have discussed the implementation of the framework of *High Energy Jets* [11, 12] in a flexible Monte Carlo; the new components discussed in the present paper include 1) the organisation of the all-order cancellation of IR divergences between real and virtual corrections (section 2.4), 2) matching to high multiplicity tree-level matrix elements (section 3), and 3) the inclusion of higher order logarithmic terms to stabilise the scale dependence (section 4).

In section 5 we studied the impact of the perturbative corrections included in *High Energy Jets* on a number of dijet and trijet distributions. We find that compared to LO, the distribution is harder in both the transverse momentum and in H_T (the scalar sum of transverse jet momenta), while the invariant-mass distribution between the two hardest jets is softened. Similar results hold for trijet-observables. Therefore, the understanding of the radiative corrections could lead to better methods for suppressing the Standard Model contribution in new-physics searches.

The effect of hard, perturbative corrections is cleanly displayed by the average number of hard jets versus the observable in question. This is particularly true for the rapidity span between the most forward/backward hard jets, which is a direct measure of the phase space available for hard radiation.

Finally, in section 5.3, we presented the prediction obtained from *High Energy Jets* of an observable sensitive to inter-jet radiation, which is currently under study by Atlas [64]. We find that the theoretical uncertainty on the quantities studied is dominated by the scale choice, while the variation induced by pdf uncertainties is completely negligible.

The generator *High Energy Jets* is available at http://cern.ch/hej.

JHEP06(2011)010

Acknowledgments

We thank Leif Lönnblad and Jeff Forshaw for interesting discussions.

A The building blocks for the regularised *High Energy Jets*-cross sections

We define here in one place the necessary building blocks to construct an amplitude in the HEJ framework:

$$\begin{aligned}\overline{\left|\mathcal{M}^{\text{reg}}_{\text{HEJ}}(\{p_i\})\right|}^2 = &\frac{1}{4\ (N_C^2-1)}\ \|S_{f_1f_2\to f_1f_2}\|^2\\ &\cdot\left(g^2\ K_{f_1}\ \frac{1}{t_1}\right)\cdot\left(g^2\ K_{f_2}\ \frac{1}{t_{n-1}}\right)\\ &\cdot\prod_{i=1}^{n-2}\left(g^2C_A\left(\frac{-1}{t_it_{i+1}}V^\mu(q_i,q_{i+1})V_\mu(q_i,q_{i+1})-\frac{4}{\mathbf{p}_i^2}\theta\left(\mathbf{p}_i^2<\lambda^2\right)\right)\right)\\ &\cdot\prod_{j=1}^{n-1}\exp\left[\omega^0(q_j,\lambda)(y_{j-1}-y_j)\right].\end{aligned}\tag{A.1}$$

Our momentum convention will be that p_A and p_B represent the momenta of the forward and backward moving initial partons respectively. The outgoing momenta of all quarks and gluons are then numbered in decreasing rapidity so p_1 is the most forward etc. We then define q_i to be the momenta which correspond to the t-channel momenta in the effective t-channel exchange picture, that is

$$q_1 = p_A - p_1, \qquad q_i = q_{i-1} - p_i \quad 2 \le i \le n-1. \tag{A.2}$$

The current pieces, $\|S_{f_1f_2\to f_1f_2}\|^2$, indicate the square of pure current-current scattering. For quarks this is

$$\|S_{qQ\to qQ}\|^2 = \left|j^-_{a1}\cdot j^-_{bn}\right|^2 + \left|j^-_{a1}\cdot j^+_{bn}\right|^2 + \left|j^+_{a1}\cdot j^-_{bn}\right|^2 + \left|j^+_{a1}\cdot j^+_{bn}\right|^2. \tag{A.3}$$

Anti-quarks are treated in the same way with $j^-_{a1}\to\bar{j}^-_{a1} = \bar{v}^-_a\gamma^\mu v^-_1$. For gluons it is more complicated as there is an overall factor for helicity conserving channels (see eq. (2.9)):

$$\begin{aligned}\|S_{qg\to qg}\|^2 = &\left(\frac{1}{2}\ \frac{1+z^2}{z}\ \left(1-\frac{1}{C_A^2}\right)+\frac{1}{C_A^2}\right)\times\\ &\times\left(\left|j^-_{a1}\cdot j^-_{bn}\right|^2 + \left|j^-_{a1}\cdot j^+_{bn}\right|^2 + \left|j^+_{a1}\cdot j^-_{bn}\right|^2 + \left|j^+_{a1}\cdot j^+_{bn}\right|^2\right)\end{aligned}\tag{A.4}$$

For this example of a backward-moving parton $z = p_n^-/p_b^-$. The result for a forward-moving gluon is the same with $p_a \leftrightarrow p_b$, $p_1 \leftrightarrow p_n$ and $z = p_1^+/p_a^+$.

Gluon-gluon scattering is the natural generalisation of what has gone before. There are now two relevant ratios $z_1 = p_1^+/p_a^+$ and $z_2 = p_2^-/p_b^-$. Then we define

$$\begin{aligned}\|S_{gg\to gg}\|^2 = &\left(\frac{1}{2}\ \frac{1+z_1^2}{z_1}\ \left(1-\frac{1}{C_A^2}\right)+\frac{1}{C_A^2}\right)\left(\frac{1}{2}\ \frac{1+z_2^2}{z_2}\ \left(1-\frac{1}{C_A^2}\right)+\frac{1}{C_A^2}\right)\times\\ &\left(\left|j^-_{a1}\cdot j^-_{bn}\right|^2 + \left|j^-_{a1}\cdot j^+_{bn}\right|^2 + \left|j^+_{a1}\cdot j^-_{bn}\right|^2 + \left|j^+_{a1}\cdot j^+_{bn}\right|^2\right)\end{aligned}\tag{A.5}$$

JHEP06(2011)010

λ (GeV)	$\sigma(2j)$ (μb)	$\sigma(3j)$ (μb)	$\sigma(4j)$ (μb)
0.2	1.58	5.90 E-2	9.6±0.1 E-3
0.5	1.58	5.93 E-2	10.1±0.1 E-3
1.0	1.59	5.95 E-2	9.7±0.2 E-3
2.0	1.61	5.99 E-2	9.2±0.2 E-3

Table 1. Exclusive n-jet cross sections for different values of the regularisation parameter λ. The errors shown are statistical — they are not shown for the $2j$ and $3j$ rates because they are smaller than the last quoted digit.

Returning to the remaining pieces of eq. (A.1), the factors K_{f_1} are straight-forward and inspired by the exact high-energy limit: $K_q = C_F$ for a quark of any flavour and $K_g = C_A$ for gluons.

The emission vertices were given in eq. (2.10):

$$\begin{aligned} V^\rho(q_i, q_{i+1}, p_A, p_B, p_1, p_n) = &- (q_i + q_{i+1})^\rho \\ &+ \frac{p_A^\rho}{2}\left(\frac{q_i^2}{p_{i+1}\cdot p_A} + \frac{p_{i+1}\cdot p_B}{p_A\cdot p_B} + \frac{p_{i+1}\cdot p_n}{p_A\cdot p_n}\right) + p_A \leftrightarrow p_1 \\ &- \frac{p_B^\rho}{2}\left(\frac{q_{i+1}^2}{p_{i+1}\cdot p_B} + \frac{p_{i+1}\cdot p_A}{p_B\cdot p_A} + \frac{p_{i+1}\cdot p_1}{p_B\cdot p_1}\right) - p_B \leftrightarrow p_n. \end{aligned} \tag{A.6}$$

The combination of the virtual corrections in section 2.3 and the regularisation in section 2.4 give the following factor in the exponential in eq. (A.1):

$$\omega^0(q_j, \lambda) = -\frac{\alpha_s N_C}{\pi} \log \frac{\mathbf{q}_j^2}{\lambda^2} \tag{A.7}$$

where the bold indicates that it is the sum of the square of the transverse components which are included in the log.

B Variations of the regularisation parameter λ

In this appendix, we show a few results to demonstrate that our conclusions are not sensitive to the chosen value of the regularisation parameter λ. This is the scale above which radiation is considered to be a real emission. The regularisation procedure is described in full in section 2.4. We again use the cuts defined in eq. (3.6) throughout.

Table 1 shows the exclusive n-jet rates for $n = 2, 3, 4$, for values of λ from 0.2–2 GeV. We can see that the changes in λ do not have a large effect, particularly for the $2j$ and $3j$ rates.

Figure 12 shows the distribution of the rapidity difference between most forward and most backward jet, Δy_{fb}, for different values of λ both for the inclusive 2-jet sample and the exclusive 3-jet sample. The differences are very small. We use $\lambda = 0.5\,\text{GeV}$ as the default.

In the HEJ framework, the number of quarks and gluons is treated as a variable and contributions are summed over n from 2 to ∞, see eq. (2.23). In practice, there is an upper cut-off on the value of n. This has a very weak dependence on λ as it stands to reason that

JHEP06(2011)010

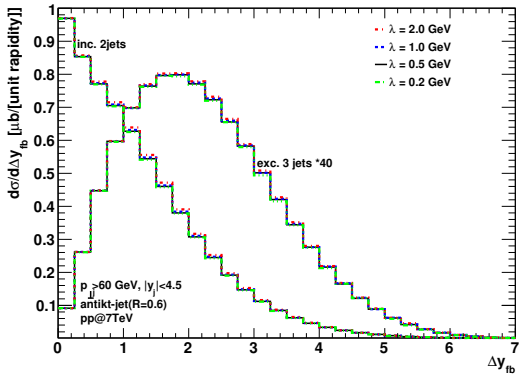

Figure 12. This plot shows the Δy_{fb} distribution, for different values of the regularisation parameter λ for the inclusive 2-jet sample and the exclusive 3-jet sample (times 40). The differences are small and we choose to use a default value of 0.5 GeV.

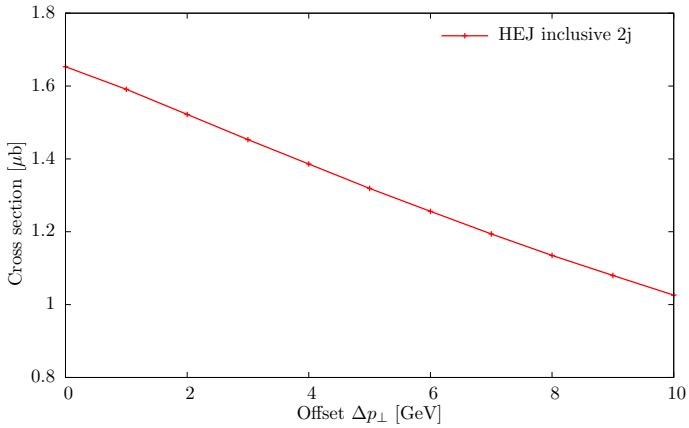

Figure 13. The inclusive dijet cross section from *HEJ* as a function of the offset-parameter $\Delta p_\perp$.

the lower the cut-off on resolved emissions, the more of them you need to consider to get the same results. For $\lambda = 0.5\,\text{GeV}$, we use $n_{\text{max}} = 22$, and find no observable difference in physical results by varying around this value.

C Stability of equal cut in the transverse momentum of dijets

As discussed in section 5.1, NLO calculations suffer from an instability when the transverse momentum cuts on the two jets are symmetric [42]. The effect is neatly demonstrated by integrating the simple BFKL approximation to the $2 \to 3$ parton matrix element,

$$\frac{|\mathcal{M}|^2}{\hat{s}^2} \propto \frac{1}{p_{1\perp}^2 p_{2\perp}^2 p_{3\perp}^2} \tag{C.1}$$

over $p_{1\perp > E_\perp + \Delta}$, $p_{2\perp > E_\perp}$ with $p_{3\perp}$ constrained by momentum conservation. The result is then propotional to (see also [30])

$$-\frac{1}{(E_\perp + \Delta)^2}\left(2\log\left(\frac{E_\perp}{E_\perp + \Delta}\right) + \frac{2E_\perp\Delta + \Delta^2}{E_\perp^2}\log\left(\frac{2E_\perp\Delta + \Delta^2}{(E_\perp + \Delta)^2}\right)\right). \tag{C.2}$$

JHEP06(2011)010

As already discussed, the $\Delta \log \Delta$-behaviour for small Δ arises because a different cut on the transverse momenta of the two hardest final state partons automatically induces a cut on the soft phase for the third final state parton. The unphysical $\Delta \log \Delta$-behaviour is solved by allowing multiple emissions from the tree-level dijet configuration, so a cut on the dijet momenta does not automatically induce a cut on the transverse momenta of further partons, and the final result obtained in HEJ has a physical behaviour. The result from *HEJ* for varying Δ, shown in figure 13, is in line with that expected from the reduction in phase space with increasing Δ.

References

[1] G. Klamke and D. Zeppenfeld, *Higgs plus two jet production via gluon fusion as a signal at the CERN LHC*, *JHEP* **04** (2007) 052 [hep-ph/0703202] [SPIRES].

[2] J.R. Andersen, K. Arnold and D. Zeppenfeld, *Azimuthal angle correlations for Higgs boson plus multi-jet events*, *JHEP* **06** (2010) 091 [arXiv:1001.3822] [SPIRES].

[3] SM and NLO Multileg Working Group collaboration, J.R. Andersen et al., *The SM and NLO multileg working group: summary report*, arXiv:1003.1241 [SPIRES].

[4] Y.L. Dokshitzer, S.I. Troian and V.A. Khoze, *Collective QCD effects in the structure of final multi-hadron states* (in Russian), *Sov. J. Nucl. Phys.* **46** (1987) 712 [*Yad. Fiz.* **46** (1987) 1220] [SPIRES].

[5] Y.L. Dokshitzer, V.A. Khoze and T. Sjöstrand, *Rapidity gaps in Higgs production*, *Phys. Lett.* **B 274** (1992) 116 [SPIRES].

[6] S. Catani, F. Krauss, R. Kuhn and B.R. Webber, *QCD matrix elements + parton showers*, *JHEP* **11** (2001) 063 [hep-ph/0109231] [SPIRES].

[7] L. Lönnblad, *ARIADNE version 4: a program for simulation of QCD cascades implementing the color dipole model*, *Comput. Phys. Commun.* **71** (1992) 15 [SPIRES].

[8] M.L. Mangano, M. Moretti and R. Pittau, *Multijet matrix elements and shower evolution in hadronic collisions: $Wb\bar{b}+n$ jets as a case study*, *Nucl. Phys.* **B 632** (2002) 343 [hep-ph/0108069] [SPIRES].

[9] S. Frixione and B.R. Webber, *Matching NLO QCD computations and parton shower simulations*, *JHEP* **06** (2002) 029 [hep-ph/0204244] [SPIRES].

[10] P. Nason, *A new method for combining NLO QCD with shower Monte Carlo algorithms*, *JHEP* **11** (2004) 040 [hep-ph/0409146] [SPIRES].

[11] J.R. Andersen and J.M. Smillie, *Constructing all-order corrections to multi-jet rates*, *JHEP* **01** (2010) 039 [arXiv:0908.2786] [SPIRES].

[12] J.R. Andersen and J.M. Smillie, *The factorisation of the t-channel pole in quark-gluon scattering*, *Phys. Rev.* **D 81** (2010) 114021 [arXiv:0910.5113] [SPIRES].

[13] J.R. Andersen, L. Lönnblad and J.M. Smillie, *A parton shower for High Energy Jets*, arXiv:1104.1316 [SPIRES].

[14] V.S. Fadin, E.A. Kuraev and L.N. Lipatov, *On the pomeranchuk singularity in asymptotically free theories*, *Phys. Lett.* **B 60** (1975) 50 [SPIRES].

JHEP06(2011)010

[15] E.A. Kuraev, L.N. Lipatov and V.S. Fadin, *Multi-reggeon processes in the Yang-Mills theory*, *Sov. Phys. JETP* **44** (1976) 443 [*Zh. Eksp. Teor. Fiz.* **71** (1976) 840] [SPIRES].

[16] E.A. Kuraev, L.N. Lipatov and V.S. Fadin, *The pomeranchuk singularity in nonabelian gauge theories*, *Sov. Phys. JETP* **45** (1977) 199 [*Zh. Eksp. Teor. Fiz.* **72** (1977) 377] [SPIRES].

[17] I.I. Balitsky and L.N. Lipatov, *The pomeranchuk singularity in quantum chromodynamics*, *Sov. J. Nucl. Phys.* **28** (1978) 822 [*Yad. Fiz.* **28** (1978) 1597] [SPIRES].

[18] J.R. Andersen and A. Sabio Vera, *Solving the BFKL equation in the next-to-leading approximation*, *Phys. Lett.* **B 567** (2003) 116 [hep-ph/0305236] [SPIRES].

[19] J.R. Andersen and A. Sabio Vera, *The gluon Green's function in the BFKL approach at next-to-leading logarithmic accuracy*, *Nucl. Phys.* **B 679** (2004) 345 [hep-ph/0309331] [SPIRES].

[20] J.R. Andersen and C.D. White, *A new framework for multijet predictions and its application to Higgs boson production at the LHC*, *Phys. Rev.* **D 78** (2008) 051501 [arXiv:0802.2858] [SPIRES].

[21] J.R. Andersen, V. Del Duca and C.D. White, *Higgs boson production in association with multiple hard jets*, *JHEP* **02** (2009) 015 [arXiv:0808.3696] [SPIRES].

[22] J.R. Andersen and J.M. Smillie, *All-order corrections and multi-jet rates*, PoS(RADCOR2009)019 [arXiv:1001.4463] [SPIRES].

[23] J.R. Andersen and J.M. Smillie, *High energy description of processes with multiple hard jets*, *Nucl. Phys. Proc. Suppl.* **205-206** (2010) 205 [arXiv:1007.4449] [SPIRES].

[24] V.N. Gribov and L.N. Lipatov, *Deep inelastic ep scattering in perturbation theory*, *Sov. J. Nucl. Phys.* **15** (1972) 438 [*Yad. Fiz.* **15** (1972) 781] [SPIRES].

[25] L.N. Lipatov, *The parton model and perturbation theory*, *Sov. J. Nucl. Phys.* **20** (1975) 94 [*Yad. Fiz.* **20** (1974) 181] [SPIRES].

[26] G. Altarelli and G. Parisi, *Asymptotic freedom in parton language*, *Nucl. Phys.* **B 126** (1977) 298 [SPIRES].

[27] Y.L. Dokshitzer, *Calculation of the structure functions for deep inelastic scattering and e^+e^- annihilation by perturbation theory in quantum chromodynamics*, *Sov. Phys. JETP* **46** (1977) 641 [*Zh. Eksp. Teor. Fiz.* **73** (1977) 1216] [SPIRES].

[28] C.R. Schmidt, *A Monte Carlo solution to the BFKL equation*, *Phys. Rev. Lett.* **78** (1997) 4531 [hep-ph/9612454] [SPIRES].

[29] L.H. Orr and W.J. Stirling, *Dijet production at hadron hadron colliders in the BFKL approach*, *Phys. Rev.* **D 56** (1997) 5875 [hep-ph/9706529] [SPIRES].

[30] J.R. Andersen, V. Del Duca, S. Frixione, C.R. Schmidt and W.J. Stirling, *Mueller-Navelet jets at hadron colliders*, *JHEP* **02** (2001) 007 [hep-ph/0101180] [SPIRES].

[31] V.S. Fadin, R. Fiore, M.G. Kozlov and A.V. Reznichenko, *Proof of the multi-Regge form of QCD amplitudes with gluon exchanges in the NLA*, *Phys. Lett.* **B 639** (2006) 74 [hep-ph/0602006] [SPIRES].

[32] B.L. Combridge and C.J. Maxwell, *Untangling large p_T hadronic reactions*, *Nucl. Phys.* **B 239** (1984) 429 [SPIRES].

JHEP06(2011)010

[33] I.I. Balitsky, L.N. Lipatov and V.S. Fadin, *Regge processes in non-Abelian gauge theories* (in Russian), in *Leningrad* 1979, *Proceedings, Physics Of Elementary Particles*, Leningrad Russia (1979), pg. 109 [SPIRES].

[34] V. Del Duca, *Parke-Taylor amplitudes in the multi-Regge kinematics*, *Phys. Rev.* **D 48** (1993) 5133 [hep-ph/9304259] [SPIRES].

[35] V. Del Duca, *Equivalence of the Parke-Taylor and the Fadin-Kuraev-Lipatov amplitudes in the high-energy limit*, *Phys. Rev.* **D 52** (1995) 1527 [hep-ph/9503340] [SPIRES].

[36] A.V. Bogdan and V.S. Fadin, *A proof of the reggeized form of amplitudes with quark exchanges*, *Nucl. Phys.* **B 740** (2006) 36 [hep-ph/0601117] [SPIRES].

[37] V.S. Fadin, M.G. Kozlov and A.V. Reznichenko, *Radiative corrections to QCD amplitudes in quasi-multi-Regge kinematics*, *Phys. Atom. Nucl.* **67** (2004) 359 [*Yad. Fiz.* **67** (2004) 377] [hep-ph/0302224] [SPIRES].

[38] V.S. Fadin, *The gluon Reggeization in perturbative QCD at NLO*, hep-ph/0511121 [SPIRES].

[39] M. Cacciari, G.P. Salam and G. Soyez, *The anti-k_t jet clustering algorithm*, *JHEP* **04** (2008) 063 [arXiv:0802.1189] [SPIRES].

[40] J.R. Andersen, *On the role of NLL corrections and energy conservation in the high energy evolution of QCD*, *Phys. Lett.* **B 639** (2006) 290 [hep-ph/0602182] [SPIRES].

[41] J.R. Andersen and A. Sabio Vera, *The gluon Green's function in $N = 4$ supersymmetric Yang-Mills theory*, *Nucl. Phys.* **B 699** (2004) 90 [hep-th/0406009] [SPIRES].

[42] S. Frixione and G. Ridolfi, *Jet photoproduction at HERA*, *Nucl. Phys.* **B 507** (1997) 315 [hep-ph/9707345] [SPIRES].

[43] T. Sjöstrand, S. Mrenna and P.Z. Skands, *A brief Introduction to* PYTHIA 8.1, *Comput. Phys. Commun.* **178** (2008) 852 [arXiv:0710.3820] [SPIRES].

[44] M. Bahr et al., HERWIG++ *physics and manual*, *Eur. Phys. J.* **C 58** (2008) 639 [arXiv:0803.0883] [SPIRES].

[45] T. Gleisberg et al., *Event generation with* SHERPA 1.1, *JHEP* **02** (2009) 007 [arXiv:0811.4622] [SPIRES].

[46] J. Alwall et al., *MadGraph/MadEvent v4: the new web generation*, *JHEP* **09** (2007) 028 [arXiv:0706.2334] [SPIRES].

[47] V.S. Fadin and L.N. Lipatov, *BFKL pomeron in the next-to-leading approximation*, *Phys. Lett.* **B 429** (1998) 127 [hep-ph/9802290] [SPIRES].

[48] V.S. Fadin and L.N. Lipatov, *Next-to-leading corrections to the BFKL equation from the gluon and quark production*, *Nucl. Phys.* **B 477** (1996) 767 [hep-ph/9602287] [SPIRES].

[49] J.R. Andersen, *A closer look at the analysis of NLL BFKL*, *AIP Conf. Proc.* **792** (2005) 726 [hep-ph/0507215] [SPIRES].

[50] S. Alioli, P. Nason, C. Oleari and E. Re, *A general framework for implementing NLO calculations in shower Monte Carlo programs: the POWHEG BOX*, *JHEP* **06** (2010) 043 [arXiv:1002.2581] [SPIRES].

[51] S. Alioli, K. Hamilton, P. Nason, C. Oleari and E. Re, *Jet pair production in POWHEG*, *JHEP* **04** (2011) 081 [arXiv:1012.3380] [SPIRES].

JHEP06(2011)010

[52] H. Jung and G.P. Salam, *Hadronic final state predictions from CCFM: The hadron-level Monte Carlo generator CASCADE*, *Eur. Phys. J.* **C 19** (2001) 351 [hep-ph/0012143] [SPIRES].

[53] H. Jung et al., *The CCFM Monte Carlo generator CASCADE* 2.2.0, *Eur. Phys. J.* **C 70** (2010) 1237 [arXiv:1008.0152] [SPIRES].

[54] R.K. Ellis and J.C. Sexton, *QCD radiative corrections to parton parton scattering*, *Nucl. Phys.* **B 269** (1986) 445 [SPIRES].

[55] W.T. Giele, E.W.N. Glover and D.A. Kosower, *Higher order corrections to jet cross-sections in hadron colliders*, *Nucl. Phys.* **B 403** (1993) 633 [hep-ph/9302225] [SPIRES].

[56] W.T. Giele, E.W.N. Glover and D.A. Kosower, *The two jet differential cross-section at $O(\alpha_S^3)$ in hadron collisions*, *Phys. Rev. Lett.* **73** (1994) 2019 [hep-ph/9403347] [SPIRES].

[57] W.T. Giele, E.W.N. Glover and D.A. Kosower, *The inclusive two jet triply differential cross section*, *Phys. Rev.* **D 52** (1995) 1486 [hep-ph/9412338] [SPIRES].

[58] Z. Nagy, *Three-jet cross sections in hadron hadron collisions at next-to-leading order*, *Phys. Rev. Lett.* **88** (2002) 122003 [hep-ph/0110315] [SPIRES].

[59] Z. Nagy, *Next-to-leading order calculation of three jet observables in hadron hadron collision*, *Phys. Rev.* **D 68** (2003) 094002 [hep-ph/0307268] [SPIRES].

[60] J.R. Forshaw, A. Kyrieleis and M.H. Seymour, *Gaps between jets in the high energy limit*, *JHEP* **06** (2005) 034 [hep-ph/0502086] [SPIRES].

[61] J. Forshaw, J. Keates and S. Marzani, *Jet vetoing at the LHC*, *JHEP* **07** (2009) 023 [arXiv:0905.1350] [SPIRES].

[62] D. Colferai, F. Schwennsen, L. Szymanowski and S. Wallon, *Mueller Navelet jets at LHC — complete NLL BFKL calculation*, *JHEP* **12** (2010) 026 [arXiv:1002.1365] [SPIRES].

[63] O. Kepka, C. Marquet and C. Royon, *Gaps between jets in hadronic collisions*, *Phys. Rev.* **D 83** (2011) 034036 [arXiv:1012.3849] [SPIRES].

[64] ATLAS collaboration, *Measurement of dijet production with a jet veto in pp collisions at $\sqrt{s} = 7$ TeV using the ATLAS detector*, ATLAS-CONF-2010-085, CERN, Geneva Switzerland (2010).

[65] V.D. Barger, R.J.N. Phillips and D. Zeppenfeld, *Mini-jet veto: a tool for the heavy Higgs search at the LHC*, *Phys. Lett.* **B 346** (1995) 106 [hep-ph/9412276] [SPIRES].

[66] A.D. Martin, W.J. Stirling, R.S. Thorne and G. Watt, *Parton distributions for the LHC*, *Eur. Phys. J.* **C 63** (2009) 189 [arXiv:0901.0002] [SPIRES].

[67] R.D. Ball et al., *A first unbiased global NLO determination of parton distributions and their uncertainties*, *Nucl. Phys.* **B 838** (2010) 136 [arXiv:1002.4407] [SPIRES].

JHEP06(2011)010